


Article

# Naturally Occurring Asbestos (NOA) in Granitoid Rocks, A Case Study from Sardinia (Italy)

Federico Lucci <sup>1,\*</sup>, Giancarlo Della Ventura <sup>1,2</sup>, Alessandra Conte <sup>1</sup>, Manuela Nazzari <sup>2,3</sup>  
and Piergiorgio Scarlato <sup>2</sup>

<sup>1</sup> Department of Science, Università Roma Tre, Largo S. Leonardo Murialdo 1, 00146 Rome, Italy; giancarlo.dellaventura@uniroma3.it (G.D.V.); alessandra.conte1991@gmail.com (A.C.)

<sup>2</sup> Department of Seismology and Tectonophysics, Istituto Nazionale di Geofisica e Vulcanologia, Via di Vigna Murata 605, 00143 Roma, Italy; manuela.nazzari@ingv.it (M.N.); piergiorgio.scarlato@ingv.it (P.S.)

<sup>3</sup> Department of Earth Science, Sapienza-Università di Roma, Piazzale Aldo Moro 5, 00185 Roma, Italy

\* Correspondence: federico.lucci@uniroma3.it

Received: 12 September 2018; Accepted: 4 October 2018; Published: 10 October 2018



**Abstract:** All six minerals defined as “asbestos” by the existing regulation on asbestos hazard, i.e., actinolite, tremolite, anthophyllite, crocidolite and amosite amphiboles, and the serpentine-group mineral chrysotile are typical constituents of mafic and ultramafic magmatic rocks of ophiolitic sequences. However, little is known about the presence and distribution of naturally occurring asbestos (NOA) in plutonic felsic rocks. The Isadalu magmatic complex outcropping in central Sardinia and belonging to the post-variscan Permian volcanic cycle, is described here as an interesting occurrence of fibrous amphiboles in granitoid rocks. Field work and collected mineralogical/petrological data show that NOA fibers from the Isadalu complex belong compositionally to the actinolite-tremolite series. They were generated by metasomatic growth on pristine magmatic hornblende, at ca. 470 °C at 1 kbar, during sodic-calcic hydrothermal alteration. In terms of environmental hazard, the Isadalu complex represents a high-value case study, since the actinolite-bearing felsic rocks outcrop in a strongly anthropized area. Here, towns with local and regional strategic infrastructures (dams, pipes, hydroelectric power plants, water supply, roads) have been developed since the last century, also using the granitoid asbestos-rich stones. The aim of this study is to demonstrate that NOA and relative hazard are not univocally connected to a restricted typology of rocks. This result should be taken into account in any future work, procedure or regulation defining asbestos occurrences in natural environments.

**Keywords:** actinolite; tremolite; asbestos; granite; late variscan magmatism; Sardinia; amphibole; sodic-calcic hydrothermal alteration

## 1. Introduction

The occurrence in nature of fibrous amphiboles (anthophyllite, actinolite, tremolite, crocidolite and amosite), and chrysotile, i.e., the six silicate minerals defined by the existing regulation as “asbestos” (e.g., [1–9]) is increasingly attracting attention in environmental hazard evaluation [1,10]. In natural environments, the NOA (natural occurring asbestos) hazard arises when physical/mechanical processes produce airborne fibers that, due to their low density and small size, can be widely dispersed and, therefore, contaminate the atmosphere and water supplies e.g., [2,3] (Figure 1).

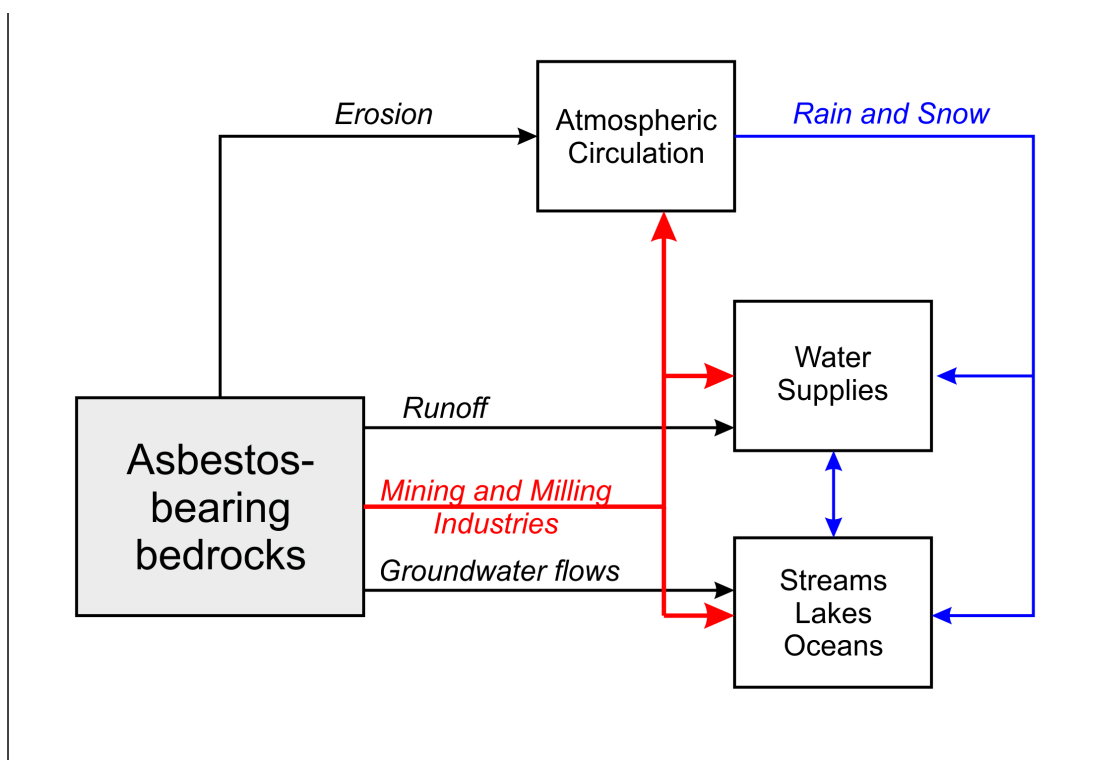


**Figure 1.** Flowchart illustrating physical/mechanical processes producing asbestos fibres distribution in the environments (modified after [3,11]).

Natural processes (erosion and transport) as well as anthropic activities (mining, crushing, grinding and milling), thus represent an important source of asbestos. Both processes may induce a strong environmental hazard [2,3,11] that can be quantified as a function of the concentration of dispersed fiber in air and in soil/water e.g., [12–18]. Up to the present, only a limited number of studies from a relatively restricted number of sites have focused on the risk produced by asbestos minerals in their natural settings [1–3]. Moreover, few works have addressed strategy and methods to quantify the concentration of asbestos in the different types of rocks [19–21].

It is recognized that asbestos minerals are typical of mafic and ultramafic rock sequences [2–4]. In these rocks, a wide range of geological processes [1–4,22], such as shear deformation and fluid-rock interaction, may produce a strong rock alteration and serpentinization, associated with a widespread growth of asbestiform amphiboles. However, despite the relevance of these occurrences and related geological phenomena, we still have a very limited knowledge (see [4] and reference therein) on the appearance and distribution of fibrous amphibole in acid rocks and specifically where Ca-inosilicates that bearing metaluminous granitoids undergo hydrothermal alteration.

In this work, we address an intriguing example of NOA in granitoid rocks from the Isadalu Permian hypabyssal felsic massif outcropping in northern Ogliastra (Central Sardinia, Italy). The Isadalu complex has been selected as a case study for a multidisciplinary approach (based on a field-survey combined with textural, mineralogical and petrological investigation) aimed at evaluating the asbestos hazard. In the studied area, fibrous amphibole-bearing granitoids have been used for centuries for house-building (a typical case of non-occupational exposure) [1], and strategic infrastructures (pipes and penstocks of the hydroelectric plants and local roads) have been developed, maintained and modernized, since the 1948 (occupational exposure) [1] (Figure 2) using these geomaterials.





**Figure 2.** The Isadalu Hbl-bearing granites in anthropic environment: (a) penstocks, Sa Teula artificial basin and watermills of the Secondo Salto hydroelectric plants; (b) eastern view of Sierra Isadalu with localization of the main infrastructures; (c) the collapsing regional Villagrande Strisaili-Talana road, built over Isadalu granites; (d) Isadalu Hbl-bearing granitoid as geomaterial: rough cut blocks used for local buildings; (e) the penstocks and their relationship with Isadalu granitoids; (f,g) Isadalu granitoid blocks used for houses and dry stone walls.

Our study demonstrates that the fibrous-amphibole hazard is not univocally related to Figure 2a specific typologies of rocks (mafic and ultramafic) [2–4,23–33] and Figure 2b fluid-rock interaction in shear-deformative metamorphic environments [2–4,23–33]. We believe that our findings could have a significant impact on future regulations defining environmental hazards connected to asbestos occurrences.

## 2. Geological Setting

The Isadalu magmatic complex is located in Ogliastra (central Sardinia) between the towns of Villagrande Strisaili and Talana. It constitutes part of the eastern flank of the Bau-Muggeris valley, located at the southeastern slope of the Gennargentu massif. The Isadalu magmatic complex belongs to the so-called “Permian volcanics” cycle (e.g., [34]) affecting the Sardinia and Corsica basement right after the variscan orogeny e.g., [34–38] (Figure 3).

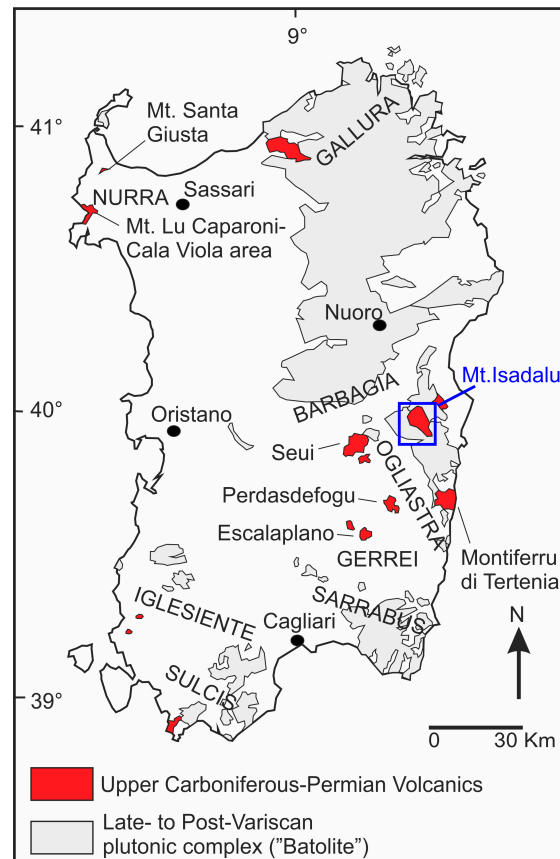


**Figure 3.** Simplified geological map of Sardinia showing the location of upper Paleozoic magmatic rocks of “Sardinia Batholith” and “Permian volcanic cycle” (modified after [38]). The blue rectangle indicates the Isadalu magmatic complex.

The Sardinia crystalline basement represents one of the southernmost segments of the European variscan collisional belt; it shows [37,38] a complete orogenic structure, from high-grade metamorphic units of the axial zone to the north, to sedimentary basins of the external zone, to the southwest [39–41]. Variscan crystalline basement of Sardinia and Corsica maybe the result of orogenic processes dated at 350–300 Ma [37–42], followed by a transition from collisional compressive to post-collisional tensional regime due to gravitative re-equilibration of the orogenic belt [37,43]. During this post-collisional phase, mainly characterized by extensional tectonics and strike-slip faulting episodes [35,39,40,44], extensive magmatism developed throughout the Sardinia-Corsica basement [34–38,41,45–47]. According to radiometric data from the existing literature [34,37,41,45–60], the late- to post-collisional magmatism widespread in the variscan basement spans from 310 to 280 Ma for major granitoid bodies (i.e., “Sardinia Batholith”) and from 290–260 Ma for basaltic and rhyolitic volcanism. Alkali-basaltic dyke swarms recognized mainly in northern Sardinia and Corsica, with ages of ca. 250–230 Ma [35,37,57–62] are interpreted as the tail of the basaltic and rhyolitic post-collisional magmatic phase [57,60–62].



“Permian volcanics” belong to the post-variscan magmatic event (e.g., [34,35,57,61,62]) and outcrop extensively from northern (Gallura and Nurra) to central (Barbagia, Ogliastra, Gerrei) down to the southern (Iglesiente-Sulcis) Sardinia [34,36,38]. Permian volcanic complexes are mainly constituted by hypabyssal and extrusive rocks, associated with widely diffused dyke swarms. These complexes intrude variscan metamorphic rocks as well as granodiorites and monzonites of the variscan Sardinia batholith e.g., [35,57]. Their volcanic activity generally began with acid explosive products associated with andesitic lavas and dykes and was followed by the emplacement of dacitic (Perdasdefogu complex in Ogliastra) and rhyolitic dykes and ignimbrites (Barbagia and Ogliastra complexes) [38,63]. In many cases, such as in Seui (Ogliastra), felsic hypabyssal domes were emplaced during the volcanic activity ([38,45,57,60,62] and references therein).

The Isadalu magmatic complex, formerly Talana-Villagrande Strisaili volcanics [34–36,45,57,60,64], is located in northern Ogliastra and represents an interesting, although poorly known, example of the late variscan Permian volcanic complex. It consists of a continuous series of mafic to felsic hypabyssal stocks, widespread dyke swarms, hydrothermal quartz veins and volcanic extrusive and explosive rocks [65–68]. Locally, in the Bau Muggeri valley, mixed sulphides (“Bau Aradulu” locality), iron oxides (“ex Miniera Zia Penneros” at Mnt. Mela, and “Corgiale” locality) and fluorite (“Martana” locality) deposits, associated to dyke swarms are also reported [65] (Figure 4).

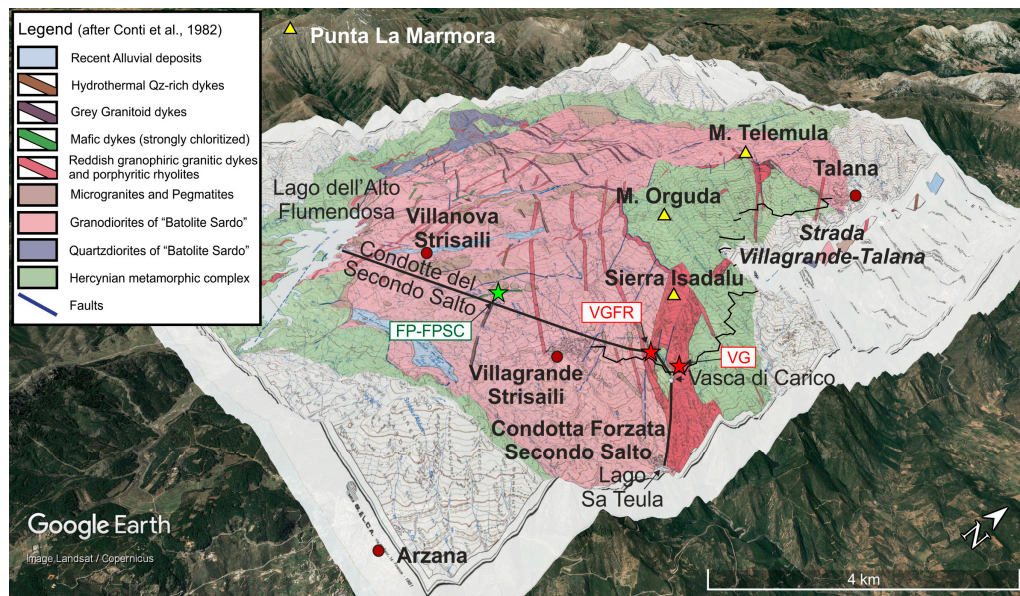


**Figure 4.** Local geological context. 3D-view of satellite image of Isadalu magmatic complex in Sardinia (Image Landsat/Copernicus from Google Earth Pro, Map Data, Google; courtesy of Google). The modified geological map [65] of the area is here reported after georeferentiation in Google Earth Pro (courtesy of Google). Punta La Marmora stands for Gennargentu massif. Green and red stars indicate sampling localities for mafic and granitoid rocks, respectively. Towns and main infrastructures of the Flumendosa hydroelectric plants are also shown.

Concerning the Isadalu magmatic complex, recent studies [66–68] focused on the main hornblende-bearing pink hypabyssal granitoid intrusion constituting the Serra Isadalu mountain and its associated aplitic and rhyolitic dyke swarms. Diffuse rhyodacitic and dacitic grey porphyroid bodies and stocks are distributed in the triangular area between Villagrande Strisaili to the south, Talana to the north and Alto Flumendosa Lake to the west [65,67,68]. Aphyric to porphyritic mafic dykes are also present along Bau Muggeris valley [65,67,68]. Near Villagrande Strisaili town a hornblende-bearing porphyritic mafic dyke [66–68] has finally been reported.

During field-survey, we observed strong hydrothermal alteration affecting Isadalu magmatic rocks (Figure 5) as testified by (i) fractures showing hydrothermal haloes, (ii) diffuse hydrothermal-to-

pneumatolithic meso- to macro-crystalline quartz veins, (iii) widespread systems of chlorite-epidote veinlets (mainly in felsic rocks), (iv) strong albitization phenomena, and (v) pseudomorphic growth of fibrous amphiboles over the pristine magmatic hornblende.

During the geological campaign, fibrous amphibole-bearing magmatic rocks were observed and mapped across the entire area from southern Gennargentu massif (“Ruinas” locality) down to Monte Cartucceddu (“MontiFerru di Tertenia” area) on the eastern coast, covering ca. 100–120 square kilometers. These findings are consistent with documented occurrences of actinolite in late-hercynian rocks outcropping in mid-eastern Sardinia [37].

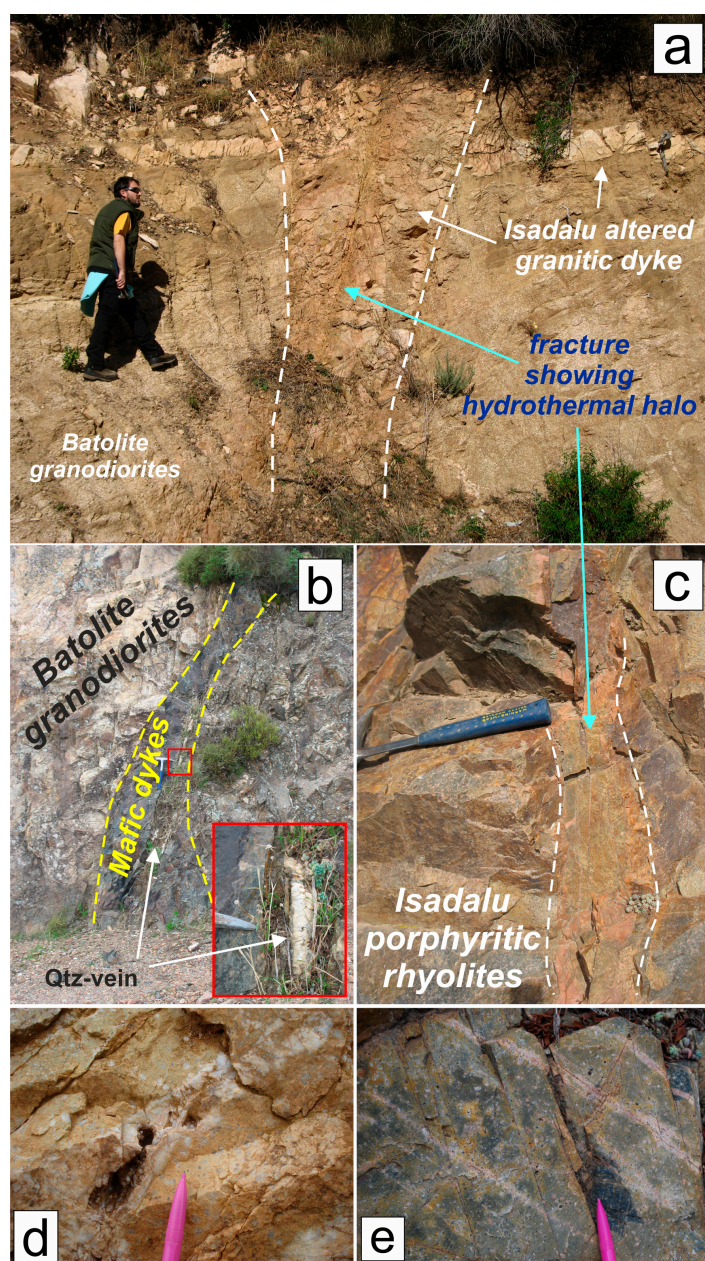


**Figure 5.** Field photographs of veins and hydrothermal fractures in Isadalu magmatic complex: (a) major fracture showing hydrothermal halo cutting metric Isadalu granitoid dyke; (b) mafic dyke cut by late Qtz-vein, in the red rectangle a close-up field photograph; (c) fracture with hydrothermal halo in Isadalu porphyritic rhyolites; (d) late Qtz-vein cutting the Isadalu granitoid body; (e) Ep + Chl veins with associated alteration halo, cutting the Isadalu porphyritic rhyolites.



### 3. Materials and Methods

One mafic and two felsic samples representative of main NOA-bearing magmatic lithologies from the area of Isadalu complex were selected for petrographic investigations and mineral chemistry on polished thin sections. We excluded at this stage to investigate samples from both the “Gennargentu National Park” and “MontiFerru Regional Nature Reserve” where no anthropic activity is allowed.

Rock fabric and amphibole texture were studied using a Nikon Eclipse 50iPol polarized-light microscope (PLM, Nikon, Tokyo, Japan) equipped with Nikon Ds-Fi2 CCD camera (Nikon, Tokyo, Japan) at Laboratory of Microtectonics, Department of Science, University of Roma TRE. Images from polished thin section were acquired using the Nikon Nis-Elements software (Ver4.30.01, Nikon, Tokyo, Japan). Mineral compositions were analyzed by combined WDS–EDS techniques using a Jeol JXA 8200 electron microprobe (EMPA, Jeol, Tokyo, Japan) at High-Pressure-High-Temperature Laboratory of Experimental Geophysics and Volcanology, Department of Seismology and Tectonophysics, INGV, Rome. Operating conditions were 15 keV and 7.5 nA, counting times of 10 s and 5 s on peaks and background, respectively, focused beam with beam size of 2.5  $\mu\text{m}$ . Compositions were determined relative to natural and synthetic standards.

Backscattered electron (BSE) images were obtained by using the same electron microprobe operating as a high-resolution scanning electron microscope (SEM). Operating conditions for BSE images acquisition were 15 keV, 7.5 nA. Optical determination on amphiboles were based on the mineralogical tables of W.E. Tröger [69]. Feldspar structural formulae were calculated using the CalcMin\_32 excel spreadsheet [70]. Chlorite structural formula were calculated following the stoichiometric criteria proposed by Vidal et al. [71]. Amphibole formula were calculated through the ACES2013 excel spreadsheet [72]. Mineral abbreviations are after the work of Whitney and Evans [73].

### 4. Results

#### 4.1. Petrography

Hereafter, we present a description of the primary magmatic fabric and texture of analyzed rocks, and the secondary unoriented (i.e., isotropic) overgrowth of the acicular amphibole + chlorite + epidote + albite (Amph + Chl + Ep + Ab) paragenesis. Moreover, following the guidelines proposed in Gunter et al. [1], we examined the habit and morphology of the actinolite/tremolite overgrowth with two independent methods based on the use of (i) a polarizing-light microscope and (ii) a scanning electron microscope.

##### 4.1.1. Primary Magmatic Fabric

The Isadalu magmatic complex is composed of felsic hypabyssal dykes, stocks and minor extrusive bodies associated with mafic dykes. The outcropping rocks display porphyritic to oligophyric and aphyric textures with isotropic to fluidal fabrics (Figure 6).

Mafic dykes show oligophyric meso- to micro-crystalline near-isotropic textures (Figure 6a) dominated by euhedral plagioclase (Pl  $\approx$  30 vol%) with minor alkali-feldspar (Afs < 10 vol%) phenocrysts. Locally, plagioclase phenocrystals orientation indicates the magmatic anisotropy of these bodies. Euhedral to subhedral hornblende (Hbl up to 30 vol%), biotite (Bt  $\approx$  5–10 vol%) and epidote (Ep < 5 vol%) constitutes the mafic phenocryst assemblage. Accessory minerals are Al-Cr-spinel (Al-Cr-Spl), ilmenite (Ilm), sphene (Spn), and rutile (Rt). The groundmass is microcrystalline ophitic, and its mineralogical assemblage includes plagioclase (Pl  $\approx$  50–60 vol%) + hornblende (Hbl  $\approx$  10–20 vol%) + biotite (Bt  $\approx$  10 vol%). Following the simplified QAPF (modal Quartz, Alkali feldspar, Plagioclase, Feldspathoid (Foid)) version for plutonic rocks [74–77], on the basis of the mineral mode these mafic rocks can be classified as dioritoid with meso- to melano-cratic character [74–77]. Considering the conspicuous abundance of hornblende associated to plagioclase and orthoclase, these rocks could be furtherly named “Appinite” [4,74].



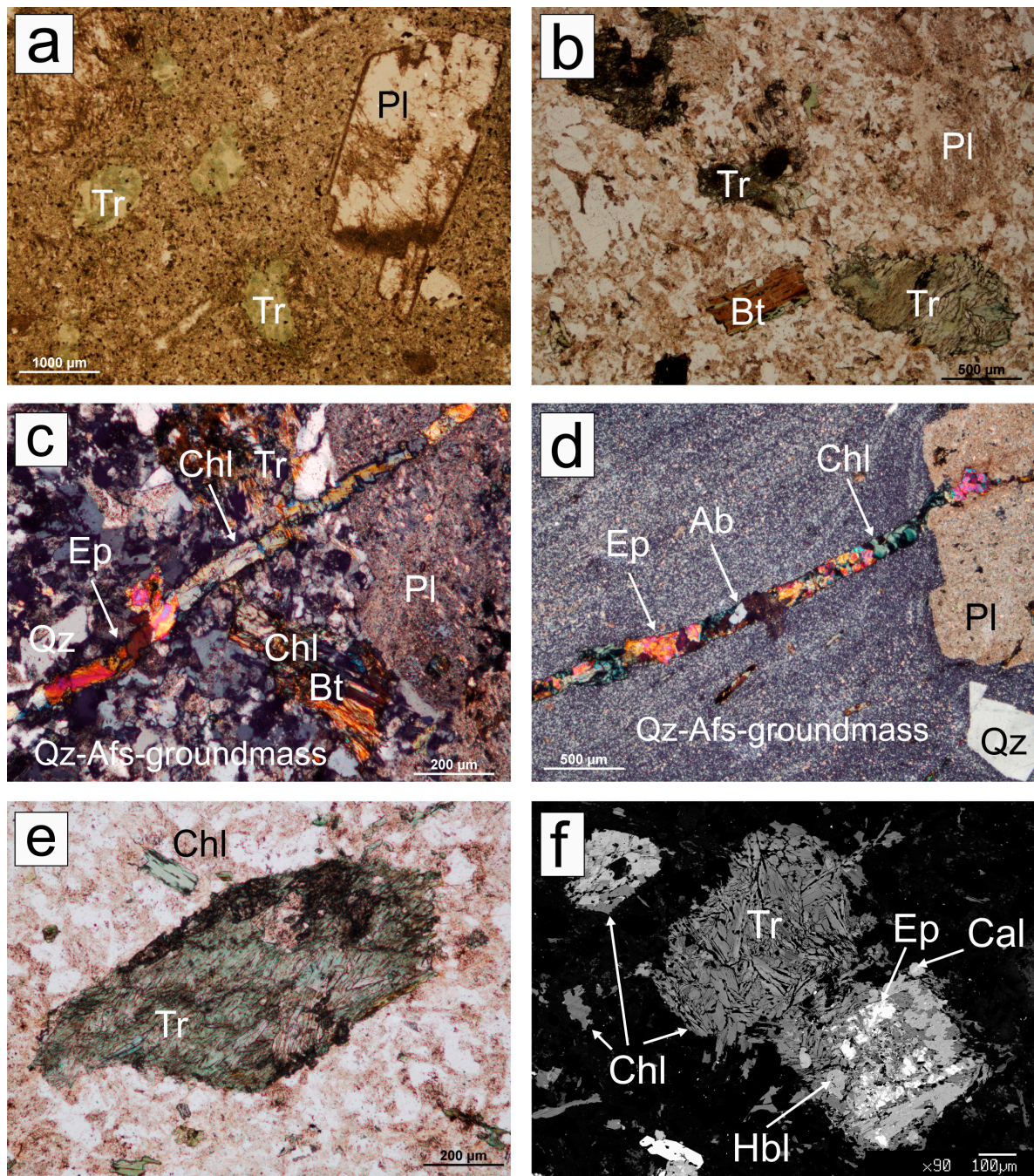


**Figure 6.** Thin section and back-scattered electron (BSE) images of the Isadalu magmatic rocks: (a) albitized plagioclase and hornblende with pseudomorph textures in mafic oligophyric dykes; (b) albitized plagioclase, chloritized biotite and hornblende with pseudomorph texture in porphyritic felsic rock; (c,d) Isadalu felsic rocks showing holocrystalline meso- to micro-crystalline textures and isotropic to fluidal fabrics; Chl + Ep veinlets are commonly observed in felsic rocks; (e) PLM image showing acicular amphibole pseudomorphosis on primary hornblende; (f) BSE image showing secondary assemblage (Tr + Chl + Ep + Cal) pseudomorphosis on Hbl + Pl.

Felsic rocks from the main Isadalu complex body (i.e., Sierra Isadalu) are represented by porphyritic hypabyssal pink plutonic rocks crossed by gray to pink extrusive/subvolcanic dykes. The fabric of these felsic rocks varies from isotropic to fluidal (Figure 6b–d). Assemblages are dominated by quartz (Qz  $\approx$  15 vol%), plagioclase (Pl  $\approx$  10–20 vol%), hornblende (Hbl  $\approx$  10–20 vol%), biotite (Bt  $\approx$  5–10 vol%), epidote (Ep  $<$  5 vol%) and sphene (Spn  $<$  5 vol%). The groundmass is holocrystalline



autoalotriomorphic, meso-crystalline to micro-crystalline and is mainly constituted by Qz + Afs with eutectic texture (Figure 5c–d). Using the simplified QAPF scheme the pink hypabyssal rocks can be classified as granitoids, while the extrusive gray to pink dykes can be named as “rhyolitoids”. All felsic rocks show leuco- to meso-cratic character [74–77]. Considering the scheme proposed by Shand [78–80] based on primary phases, the assemblage Hbl + Ep + Bt + Spn + Pl qualitatively suggests a mean metaluminous signature for the Isadalu magmatic complex rocks. This result agrees with existing works [66–68], where preliminary whole rock geochemistry highlighted a metaluminous calc-alkaline signature.

#### 4.1.2. Secondary Fabric

The studied mafic and felsic magmatic rocks show a pervasive and diffuse sub-solidus secondary isotropic (i.e., unoriented) crystallization phase characterized by acicular amphibole + chlorite + epidote + albite.

In particular, it is possible to observe (i) a severe albitization of plagioclase feldspars (Figure 6a–d), (ii) chloritization of biotite and genesis of chlorite at the expense of magmatic amphibole (Figure 6a–f), (iii) formation of a second generation of epidote on both calcic plagioclase and primary hornblende (Figure 6c,d,f); (iv) diffuse acicular amphibole pseudomorphosis on primary hornblende (Figure 6a,b,e,f). Locally, together with epidote, minor crystals of calcite were observed. In addition, felsic rocks are characterized by the presence of millimetric to sub-millimetric veins of neofomed Chl + Ep ± Ab (Figure 6c,d). These veins are invariably amphibole-free.

#### 4.1.3. Secondary Amphibole Morphology

Since the term “asbestos” is, by definition, related to the shape of the mineral particles, we carefully investigated by PLM and SEM the morphology of the secondary amphiboles in both mafic and felsic rocks (Figures 6 and 7).

Polarized-light microscopy has been widely used in the past for the definition of asbestos in a regulatory field [1] and it is still widely used as a primary technique [1,81,82] because it permits to determine, in thin section, the mineral’s morphology and the identity of particles from few millimeters to about 1  $\mu\text{m}$ . Scanning electron microscopy is not considered part of the asbestos regulatory discipline [1]; however, it permits to study particles at a resolution down to 0.1  $\mu\text{m}$  [1]. Optical characteristics from PLM observations were determined to discriminate and define the secondary amphibole identity on a preliminary basis; as a second step, integration of PLM and SEM investigations were used to describe the secondary amphibole morphology and recognize possible asbestiform/fibrous habits (Figure 7).

Secondary amphiboles, in both mafic and felsic rocks, show acicular-fibrous (elongated parallel to c crystallographic axis) to flaky morphology. Extinction is oblique (extinction angles measured  $X^a = 3\text{--}5^\circ$  and  $Z^c$  up to  $10^\circ$ ; Y is parallel to b) and elongation is positive. In thin section, these amphiboles vary from colorless to pleochroic (X = pale green/pale yellowish green; Z = light bluish green). Optical relief is always positive, as determined by Becke line test with respect to calcic-plagioclase and quartz. Birefringence varies from 0.015–0.020. Optical determinations permit to define the secondary amphibole as actinolite-tremolite (Act/Tr). For a positive mineral identification and characterization, major element compositions were investigated by EMPA.

Concerning the secondary amphibole morphology, the actinolite-tremolite material in the Isadalu rocks is recognized (Figure 7a–f) as elongated crystals, aggregate clusters, elongated flakes, bundles, fibers and solitary needles. At higher magnifications, it is possible to note that elongated crystals, at their frayed ends or where fractured, are constituted of acicular to fibrous aggregates (Figure 7e). Actinolite-tremolite fibers show widths from 2  $\mu\text{m}$  down to  $<1 \mu\text{m}$ , with lengths from 10–20  $\mu\text{m}$  to more than 200  $\mu\text{m}$ . In particular, elements showing widths  $\leq 1 \mu\text{m}$  present a very high length-to-width ratio (i.e., aspect ratio A.R.: length divided by width) [2,3] from 10:1 to higher than 20:1. Thus, these amphiboles could be defined as asbestos on the basis of the criteria of Harper et al. [83] and

Chatfield [84]. Secondary amphibole shows equilibria relationship with albite feldspars and their growth appears to be prior to chlorite + secondary epidote growth.

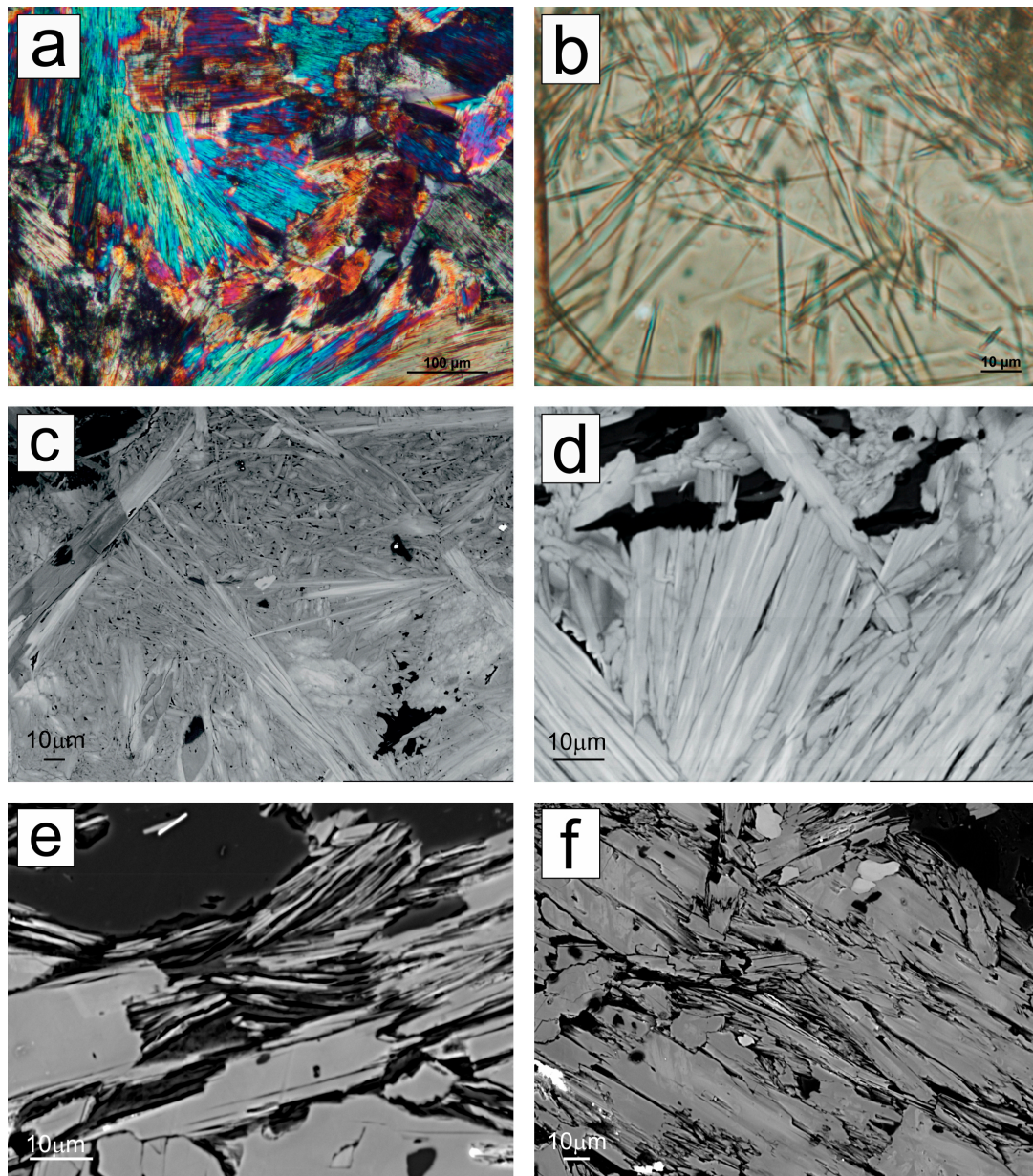


**Figure 7.** Thin section and back-scattered electron (BSE) images of the secondary amphibole in Isadalu magmatic rocks: (a,b) PLM images (crossed and parallel polarizers) of secondary amphibole pseudomorphosis; (c,d) BSE images showing geometry and morphology of secondary amphiboles; (e,f) BSE images of secondary amphibole with frayed ends showing acicular to fibrous aggregates morphology.

#### 4.2. Mineral Chemistry

Phases constituting primary magmatic assemblages and secondary overgrowths from both mafic andesite and felsic granitoid rocks were analyzed to investigate their chemistry. Representative mineral compositions and formulae, as obtained from electron microprobe analyses, and used for inverse thermobarometric estimates [85–99], are discussed below. The complete dataset is given in the supplementary material (Tables S1–S4).



#### 4.2.1. Feldspar

In andesite rock, feldspars are predominantly plagioclase with anorthite in the range  $X_{An} = 42\text{--}68\%$ . Major phenocrysts show normal zonation with labradorite to bytownite cores ( $X_{An} = 70\text{--}81\%$ ). Orthoclase component is always minor than 5% (mean value 2%). Very rare specimen of alkali-feldspar ( $Ab_{2-7}Or_{93-98}$ ) are also present.

In granite, primary feldspar association is characterized by the presence of oligoclase plagioclase ( $X_{An} = 13\text{--}15\%$ ) and K-feldspar ( $X_{Or} = 92\text{--}96\%$ ). Both andesite and granite rocks are characterized by a diffuse presence of secondary albite ( $X_{Ab} = 90\text{--}93\%$ ). Representative results are reported in Table 1.

**Table 1.** Representative Electron Microprobe analyses and chemical formulae of feldspar from Isadalu magmatic complex.

Rock Sample	Andesite FP-FPSC				Granitoid VG-VGFR			
	Type	Primary		Secondary	Primary		Secondary	
Spot	#72	#62	#26	#42	#102	#46	#109	#138
SiO <sub>2</sub> (wt%)	48.21	54.41	66.67	66.04	66.34	64.73	68.75	67.86
Al <sub>2</sub> O <sub>3</sub>	30.96	27.36	17.48	20.40	17.54	17.44	15.17	19.29
FeO <sub>tot</sub>	0.45	0.22	0.21	0.16	0.07	0.14	0.26	0.14
CaO	16.02	10.65	0.00	2.13	3.55	0.00	2.00	1.49
Na <sub>2</sub> O	2.42	6.06	0.80	11.66	11.15	0.97	11.75	11.58
K <sub>2</sub> O	0.11	0.31	15.82	0.16	0.17	16.07	0.11	0.11
Total	98.17	99.00	100.99	100.55	98.82	99.35	98.04	100.46
Si (apfu)	2.25	2.49	3.04	2.90	2.97	3.02	3.08	2.97
Al	1.70	1.47	0.94	1.06	0.93	0.96	0.80	0.99
Fe <sup>3+</sup>	0.02	0.01	0.01	0.01	0.00	0.01	0.01	0.01
Ca	0.80	0.52	0.00	0.10	0.17	0.00	0.10	0.07
Na	0.22	0.54	0.07	0.99	0.97	0.09	1.02	0.98
K	0.01	0.02	0.92	0.01	0.01	0.96	0.01	0.01
An (%) <sup>(a)</sup>	78%	48%	-	9%	15%	-	8%	6%
Ab (%) <sup>(a)</sup>	21%	50%	7%	90%	84%	8%	91%	93%
Or (%) <sup>(a)</sup>	1%	2%	93%	1%	1%	92%	1%	1%

Total iron (FeO<sub>tot</sub>) given as FeO; apfu: atoms per formula unit. <sup>(a)</sup> Abbreviation used in table to indicate ternary feldspar compounds: An: Anorthite; Ab: Albite; Or: Orthoclase.

#### 4.2.2. Epidote

In both andesite and granitoid rocks, primary epidote occurs as euhedral to subhedral grains in contact with amphibole and biotite. Secondary epidote is mostly recognized as an alteration product of primary plagioclase and hornblende. Primary epidote is characterized by higher pistacite ( $X_{Ps}$  as atomic  $[Fe^{3+}/(Fe^{3+} + Al^{3+})]$ ) [85,86] content in the range of 23–34%, whereas secondary epidote shows lower Pistacite content ( $X_{Ps}$ : 16–21%) [85–87]. Representative results are reported in Table 2.

**Table 2.** Representative Electron Microprobe analyses and chemical formulae of epidote from Isadalu magmatic complex.

Rock Sample	Andesite FP-FPSC				Granitoid VG-VGFR			
	Type	Primary		Secondary	Primary		Secondary	
Spot	#19	#18	#164	#21	#106	#108	#82	#88
SiO <sub>2</sub> (wt%)	38.20	38.30	37.83	38.78	37.16	37.64	38.05	39.21
TiO <sub>2</sub>	0.27	0.28	0.02	0.03	0.39	1.07	0.06	0.03
Al <sub>2</sub> O <sub>3</sub>	21.35	25.10	23.12	25.98	20.95	23.75	25.54	26.43
FeO <sub>tot</sub>	14.21	10.29	8.78	7.47	14.97	11.11	9.12	7.34
MnO	0.25	0.26	0.45	0.07	0.55	0.18	0.40	0.32
MgO	0.01	0.09	0.16	0.05	0.22	0.09	0.04	0.05

Table 2. Cont.

Rock Sample	Andesite FP-FPSC				Granitoid VG-VGFR			
	Primary		Secondary		Primary		Secondary	
Spot	#19	#18	#164	#21	#106	#108	#82	#88
CaO	22.92	23.38	22.65	23.42	22.59	23.26	24.21	24.22
Na <sub>2</sub> O	0.04	0.00	0.00	0.05	0.00	0.03	0.01	0.00
K <sub>2</sub> O	0.03	0.00	0.00	0.00	0.05	0.03	0.04	0.03
Total	97.27	97.70	93.01	95.85	96.87	97.15	97.46	97.63
<i>Formula (12.5 oxygens)</i>								
Si (apfu)	3.04	3.00	3.10	3.06	2.98	2.98	2.99	3.05
Ti	0.02	0.02	0.00	0.00	0.02	0.06	0.00	0.00
Al	2.00	2.31	2.23	2.42	1.98	2.21	2.36	2.42
Cr	0.00	0.00	0.00	0.00	0.00	0.00	0.00	0.00
Fe <sup>3+</sup>	0.94	0.67	0.60	0.49	1.00	0.73	0.60	0.48
Mn <sup>3+</sup>	0.02	0.02	0.03	0.00	0.04	0.01	0.03	0.02
Mg	0.00	0.01	0.02	0.01	0.03	0.01	0.00	0.01
Ca	1.95	1.96	1.99	1.98	1.94	1.97	2.04	2.02
Na	0.01	0.00	0.00	0.01	0.00	0.00	0.00	0.00
X <sub>Ps</sub> <sup>(a)</sup>	0.32	0.23	0.21	0.17	0.34	0.25	0.20	0.16

Total iron (FeO<sub>tot</sub>) given as FeO; apfu: atoms per formula unit. <sup>(a)</sup> X<sub>Ps</sub>: Pistacite, atomic [Fe<sup>3+</sup>/(Fe<sup>3+</sup> + Al<sup>3+</sup>)] after [85–87].

#### 4.2.3. Chlorite

Two homogenous populations of chlorite have been identified in both andesite and granitoid rocks. The dominant population is constituted of neoblastic isotropic aggregates and show SiO<sub>2</sub> = 26.03–29.67 wt% with Al<sub>2</sub>O<sub>3</sub> = 12.37–19.89 wt%, FeO<sub>tot</sub> = 19.20–28.85 wt% and MgO = 11.65–19.28 wt%. K<sub>2</sub>O is always less than 0.07 wt%. The crystal-chemical formulae of chlorite have been calculated on the basis of 14 oxygens with Al<sup>3+</sup>-Fe<sup>3+</sup> substitution and Fe<sup>3+</sup>-in-Chl estimates using the stoichiometric criteria [69]; examination of results shows that Si ranges between 2.79–3.13 apfu, X<sub>Fe<sup>3+</sup></sub> between 0.06–0.36 (where X<sub>Fe<sup>3+</sup></sub> = atomic [Fe<sup>3+</sup>/(Fe<sup>3+</sup> + Fe<sup>2+</sup>)] and X<sub>Mg</sub> = 0.53–0.72 (where X<sub>Mg</sub> = [Mg/(Mg + Fe<sup>2+</sup>)]), corresponding to Al<sup>[iv]</sup> between 0.87–1.21 apfu and Al<sup>[iv]</sup> = 0.73–1.27 apfu.

A second cluster of chlorites represented by chlorite-growth on biotite phenocrystals shows SiO<sub>2</sub> content 27.57–29.94 wt% (corresponding to Si 2.92–3.11 apfu), higher FeO<sub>tot</sub> (26.07–32.72 wt%) and K<sub>2</sub>O (0.27–1.45 wt%) opposite to lower MgO (7.97–14.38 wt%) contents corresponding to a structural formula with Al<sup>[iv]</sup> in the range of 0.89–1.07 apfu and Al<sup>[vi]</sup> = 1.03–1.33 apfu. Representative results are reported in Table 3.

**Table 3.** Representative Electron Microprobe analyses and chemical formulae of chlorite from Isadalu magmatic complex.

Rock Sample	Andesite Fp-FSC				Granitoid VG-VGFR				
	Chlorite			Chloritized-Biotite	Chlorite		Chloritized-Biotite		
Spot	#55	#54	#56	#60	#96	#98	#112	#14	#16
SiO <sub>2</sub> (wt%)	26.29	27.63	28.63	29.96	29.29	28.30	26.94	27.80	29.49
TiO <sub>2</sub>	0.02	0.00	0.03	0.11	0.01	0.22	0.01	2.07	0.11
Al <sub>2</sub> O <sub>3</sub>	19.89	17.35	16.79	17.55	13.50	16.13	17.63	17.78	16.02
FeO <sub>tot</sub>	20.30	19.62	19.20	28.02	25.26	25.59	27.20	26.27	30.02
MnO	0.65	0.65	0.48	0.36	0.07	0.17	0.19	0.64	0.47
MgO	17.60	19.11	18.66	10.10	15.77	15.07	13.56	10.05	9.38
CaO	0.05	0.09	0.10	0.07	0.07	0.00	0.12	0.19	0.58
Na <sub>2</sub> O	0.03	0.07	0.04	0.02	0.02	0.00	0.00	0.07	0.11
K <sub>2</sub> O	0.03	0.01	0.00	1.75	0.00	0.00	0.00	0.45	1.09
Total	84.85	84.53	83.94	87.94	84.00	85.48	85.66	85.31	87.26

Table 3. Cont.

Rock Sample	Andesite Fp-FSC					Granitoid VG-VGFR			
	Type	Chlorite			Chloritized-Biotite	Chlorite	Chloritized-Biotite		
Spot	#55	#54	#56	#60	#96	#98	#112	#14	#16
<i>Formula (14 oxygens)</i>									
Si, (apfu)	2.79	2.92	2.99	3.10	3.13	2.97	2.85	2.95	3.11
Ti	0.00	0.00	0.00	0.01	0.00	0.02	0.00	0.16	0.01
Al	2.48	2.16	2.07	2.14	1.70	2.00	2.20	2.22	1.99
Al <sup>[iv]</sup>	1.21	1.08	1.00	0.89	0.87	1.01	1.15	0.89	0.88
Al <sup>[vi]</sup>	1.27	1.08	1.06	1.25	0.83	0.99	1.05	1.33	1.10
Fe <sup>2+</sup>	1.69	1.54	1.16	1.55	1.44	1.44	1.54	1.49	1.69
Fe <sup>3+</sup>	0.11	0.19	0.52	0.87	0.81	0.81	0.87	0.84	0.95
Mn	0.06	0.06	0.04	0.03	0.01	0.02	0.02	0.06	0.04
Mg	2.78	3.01	2.91	1.56	2.51	2.36	2.14	1.59	1.47
Ca	0.01	0.01	0.01	0.01	0.01	0.00	0.01	0.02	0.07
Na	0.01	0.01	0.01	0.00	0.01	0.00	0.00	0.01	0.02
K	0.00	0.00	0.00	0.23	0.00	0.00	0.00	0.06	0.15
X <sub>Fe<sup>3+</sup></sub> <sup>(a)</sup>	0.06	0.11	0.31	0.36	0.36	0.36	0.36	0.36	0.36
X <sub>Mg</sub> <sup>(b)</sup>	0.62	0.66	0.72	0.50	0.63	0.62	0.58	0.52	0.47
T (°C) <sup>(c)</sup> [±30 °C]	329	286	262	225	218	264	309	225	223

Total iron (FeO<sub>tot</sub>) given as FeO; apfu: atoms per formula unit. <sup>(a)</sup> X<sub>Fe<sup>3+</sup></sub> as [Fe<sup>3+</sup> / (Fe<sup>3+</sup> + Fe<sup>2+</sup>)] with Fe<sup>3+</sup>-in-Chl estimates using stoichiometric criteria [71]. <sup>(b)</sup> X<sub>Mg</sub> as [Mg / (Mg + Fe<sup>2+</sup>)]. <sup>(c)</sup> T calculated using Al<sup>[IV]</sup>-in-Chlorite thermometry [99].

#### 4.2.4. Amphibole

In Isadalu rocks, two main clusters of amphiboles have been identified. A minor first population is represented by relic cores of the primary magmatic amphibole. Almost all magmatic hornblende analyses are from the mafic rocks; only two specimens (spots #122 and #151) were recognized in felsic rocks. Amphiboles of this group are strongly altered and substituted via pseudomorphosis by secondary amphibole + chlorite + epidote. They show Al<sub>2</sub>O<sub>3</sub> ranging from 6.33 to 14.12 wt% associated with CaO ranging from 9.51 to 12.43 wt% and high FeO (7.72–18.92 wt%) content. TiO<sub>2</sub> and Na<sub>2</sub>O contents are up to 3.47 wt% and 2.26 wt%, respectively. Formula were calculated using a 13-CNK normalization scheme. Primary amphiboles belong to the calcic-amphibole group and can be classified as magnesiohornblende to pargasite (Figure 8a) [88–90].

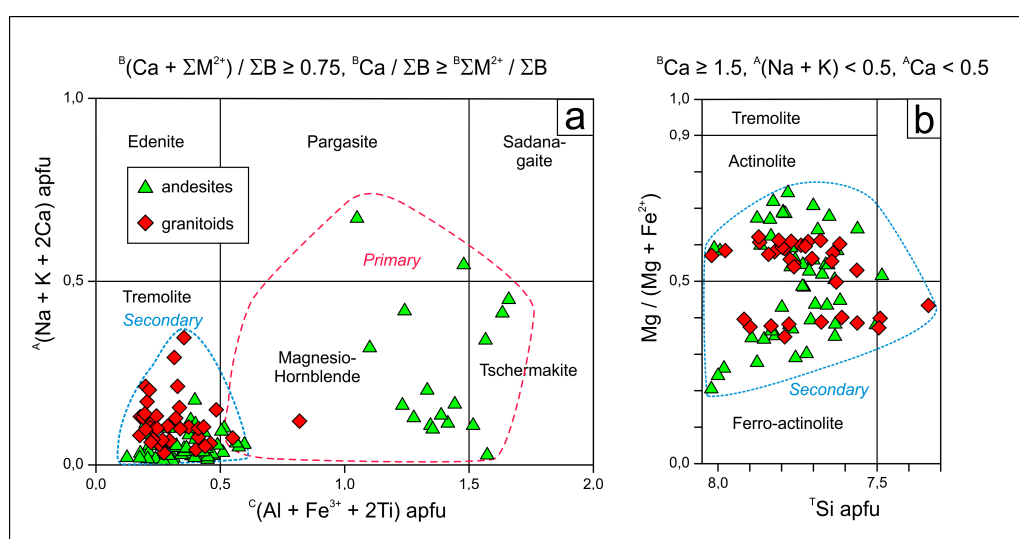


**Figure 8.** Proxy diagrams for amphibole classification [88–90], (a) calcium amphiboles and their compositional boundaries, and (b) classification diagram for amphiboles belonging to tremolite-actinolite serie.



The second population of amphiboles is dominant and is represented by secondary fibrous amphiboles. These amphiboles show lower Al<sub>2</sub>O<sub>3</sub> (0.6–5.32 wt%), opposite to higher CaO (11.31–12.95 wt%) and FeO (10.43–27.57 wt%) and belongs to the calcic group [88–90]. In particular, considering the #Mg (atomic ratio: Mg/[Mg + Fe<sup>2+</sup>]) in the range 0.20–0.74 and Si > 7.5 apfu, these amphiboles can be classified as actinolite and ferro-actinolite (Figure 8a,b) [88–90]. Representative results are reported in Table 4.

**Table 4.** Representative Electron Microprobe analyses and chemical formulae of amphiboles from Isadalu magmatic complex.

Rock Sample	Andesite FP-FPSC						Granite VG-VGFR				
	Type	Primary			Secondary			Primary		Secondary	
Spot	#9	#90	#7	#155	#166	#81	#122	#151	#116	#129	#89
SiO <sub>2</sub> (wt%)	46.61	42.34	47.35	52.81	51.99	50.86	51.59	50.28	52.96	49.50	51.93
TiO <sub>2</sub>	0.98	3.47	1.30	0.21	0.00	0.00	0.07	0.25	0.08	0.14	0.02
Al <sub>2</sub> O <sub>3</sub>	10.09	11.61	7.57	1.74	3.15	4.15	3.47	6.33	2.44	4.41	1.90
FeO <sub>tot</sub>	16.11	12.48	17.30	15.73	22.93	18.35	16.64	11.44	15.84	23.12	23.70
MnO	0.46	0.18	0.47	0.50	1.14	0.92	0.08	0.18	0.16	0.17	0.12
MgO	9.86	13.28	12.23	12.53	6.61	9.89	12.84	15.18	12.77	7.66	8.02
CaO	9.51	11.46	10.45	11.76	11.60	11.70	11.72	11.83	12.03	12.02	12.08
Na <sub>2</sub> O	1.47	2.13	1.22	0.23	0.17	0.23	0.57	0.78	0.45	0.89	0.25
K <sub>2</sub> O	2.21	0.79	0.57	0.04	0.16	0.26	0.37	0.40	0.16	0.41	0.27
Total	97.29	97.74	98.46	95.55	97.75	96.36	97.35	96.67	96.89	98.32	98.29
<i>Normalization Scheme: 13-CNK</i>											
Si, apfu	6.90	6.18	6.81	7.87	7.86	7.63	7.55	7.24	7.80	7.49	7.83
Al	1.10	1.82	1.19	0.13	0.15	0.37	0.45	0.76	0.20	0.51	0.17
ΣT	8.00	8.00	8.00	8.00	8.00	8.00	8.00	8.00	8.00	8.00	8.00
Ti	0.11	0.38	0.14	0.02	-	-	0.01	0.03	0.01	0.02	0.00
Al	0.66	0.18	0.10	0.17	0.42	0.37	0.15	0.32	0.22	0.28	0.17
Fe <sup>3+</sup>	0.36	0.54	1.14	0.09	-	0.12	0.39	0.45	0.01	-	-
Mn <sup>2+</sup>	0.06	0.02	0.06	0.06	0.15	0.12	0.01	0.02	0.02	0.02	0.02
Fe <sup>2+</sup>	1.63	0.99	0.94	1.87	2.90	2.18	1.65	0.93	1.94	2.93	2.99
Mg	2.18	2.89	2.62	2.78	1.49	2.21	2.80	3.26	2.80	1.73	1.80
ΣC	5.00	5.00	5.00	5.00	4.95	5.00	5.00	5.00	5.00	4.97	4.98
Ca	1.51	1.79	1.61	1.88	1.88	1.88	1.84	1.83	1.90	1.95	1.95
Na	0.42	0.21	0.34	0.07	0.05	0.07	0.16	0.18	0.10	0.05	0.05
ΣB	1.93	2.00	1.95	1.94	1.93	1.95	2.00	2.00	2.00	2.00	2.00
Ca	-	-	-	-	-	-	-	-	-	-	-
Na	-	0.40	-	-	-	-	-	0.04	0.03	0.21	0.03
K	0.42	0.15	0.10	0.01	0.03	0.05	0.07	0.07	0.03	0.08	0.05
ΣA	0.42	0.54	0.10	0.01	0.03	0.05	0.07	0.12	0.06	0.29	0.08
O (non-W)	22.00	22.00	22.00	22.00	22.00	22.00	22.00	22.00	22.00	22.00	22.00
W (OH)	2.00	2.00	2.00	2.00	2.00	2.00	2.00	2.00	2.00	2.00	2.00
Σ(T, C, B, A)	15.35	15.54	15.06	14.95	14.91	15.00	15.07	15.12	15.06	15.26	15.06
Species <sup>(a)</sup>	MgHbl	MgHbl	Tschk	Act	Fe-Act	Act	MgHbl	MgHbl	Act	Fe-Act	Fe-Act
Al <sub>tot</sub>	1.76	2.00	1.28	0.31	0.56	0.73	0.60	1.08	0.42	0.79	0.34
P kbar <sup>(b)</sup> [±0.5 kbar]	4.2	5.1	2.6	0.7	1.0	1.3	1.1	2.0	0.8	1.4	0.7
T (°C) <sup>(c)</sup> [±30 °C]				505	431	416			495	493	489

Total iron (FeO<sub>tot</sub>) given as FeO; apfu: atoms per formula unit. <sup>(a)</sup> Abbreviation used in table: magnesio-hornblende (MgHbl), tschermakite (Tschk), actinolite (Act), ferro-actinolite (Fe-Act). <sup>(b)</sup> Al-in-hornblende (Al-in-Hbl) barometry [97]. <sup>(c)</sup> Pl-Hbl thermometry [98] calculated for secondary amphibole at P derived by Al-in-Hbl barometry and Ab = 93%.

## 5. Thermobarometric Estimates

In order to constrain the thermobaric environment associated with the crystallization of the whole secondary paragenesis, we integrated inverse thermobarometers based on major element chemistry on Act + Pl and Chl phases. Results obtained for inverse thermobarometry models are treated using the “weighted average” routine in ISOPLOT4.1 excel spreadsheet [91] and discussed following the statistical approach proposed in Calzolari et al. [92].

Inverse thermobarometry calculations, based on both Al-in-hornblende barometry [93–97], and hornblende-plagioclase thermometry [94,96,98], have been performed using EXCEL 2010 (Microsoft, Redmond, WA, USA). Representative results are shown in Table 4.

Secondary actinolite compositions, with  $\text{Al}_2\text{O}_3$  ranging between 0.6 and 5.32 wt%, corresponding to  $\text{Al}_{\text{tot}}$  0.11–0.95 apfu (mean value: 0.52 apfu), provide  $P = 0.55\text{--}1.70 \pm 0.5$  kbar, with a weighted mean value of  $0.98 \pm 0.10$  kbar (Al-in-Hbl barometry:  $1\sigma = 10\%$ , MSWD = 0.27,  $n = 92$ , confidence = 95%) and  $T = 390\text{--}540 \pm 30$  °C, with a weighted mean value of  $466 \pm 8$  °C (Pl-Hbl thermometry for An = 7% in secondary albite:  $1\sigma = 1.8\%$ , MSWD = 1.7,  $n = 87$ ; reject = 1, confidence = 95%). Higher pressures (ca. 2–7 kbar) are instead obtained for primary magmatic hornblendes.

Inverse thermometry has been based on the  $\text{Al}^{\text{IV}}$ -in-chlorite [99] derived from compositions of chlorites and chloritized-biotite. Chlorite compositions indicate temperature values of 218–328  $\pm$  30 °C, with a weighted mean value of  $273 \pm 15$  °C ( $1\sigma = 5.3\%$ ; MSWD = 0.90,  $n = 17$ , confidence = 95%). Chlorite overgrowth on biotite (i.e., chloritized biotite) yield comparable temperatures (223–284  $\pm$  30 °C) with a weighted mean value of  $245 \pm 20$  °C ( $1\sigma = 8.0\%$ ; MSWD = 0.48,  $n = 9$ , confidence = 95%).

Collectively, the P-T conditions obtained by inverse thermobarometry, suggest a solid-state isotropic temperature-driven crystallization at superficial condition (ca. 1 kbar) with temperature peak in the window 390–540 °C and tail at ca. 220–320 °C. Assuming an average crustal density of 2700 kg/m<sup>3</sup> (e.g., [100]), this scenario evolved at a crustal depth of 3–4 km.

## 6. Discussion

The Isadalu magmatic complex belongs to the Permian volcanic cycle affecting the Paleozoic Sardinia basement right after the variscan orogeny [34–62]. It is constituted of a continuous series of mafic to felsic rocks from hypabyssal intrusions, dyke swarms and extrusive volcanics products. As already recognized in most of the late variscan calc-alkaline dykes of mid-eastern Sardinia [37], Isadalu magmatic rocks show hornblende-bearing primary assemblages, with hornblende up to 20–30% in volume, indicating a metaluminous signature in agreement with existing geochemical data [66–68]. Local actinolite pseudomorphosis on Ca-inosilicates, such as hornblende [37] and clinopyroxene [37], has been already reported [37,101] in many of the late hercynian (variscan) mafic oligophyric dykes in mid-eastern Sardinia (Ogliastro, Gerrei and Barbagia).

However, with respect to late hercynian calc-alkaline complexes of mid-eastern Sardinia [37], the most notable feature of the Isadalu magmatic complex is the presence of secondary tremolite-actinolite amphiboles also in the hypabyssal acidic granitoid rocks. Petrographic investigations (PLM and SEM), described here, highlighted that actinolite-tremolite amphiboles (i) grew as isotropic unoriented pseudomorphosis over primary hornblende, (ii) are characterized by an acicular to fibrous morphology (width  $\leq 1$   $\mu\text{m}$  and A.R. from 10:1 to higher than 20:1) compatible with the “asbestos” definition [83,84], (iii) show equilibria relationships with albite-forming on plagioclase and (iv) show a pre- to syn-character with respect to secondary chlorite + epidote.

### 6.1. Genesis of Actinolite-Tremolite

Fabric observations, in both mafic and felsic rocks, allow recognizing a scenario of a secondary NOA-bearing paragenesis superimposed over a pristine primary magmatic assemblage. Furthermore, the invariably isotropic fabric of this secondary paragenesis, together with its widespread diffusion in the studied rocks clearly indicates that the secondary minerals were not related to shear-deformative processes, development of metamorphic foliation, and fluid-rock interaction along fault planes [2,3,102–104]. The fabrics observed in the Isadalu rocks, instead, describes deformation-free (isotropic fabrics) and fluid-rich (chlorite-epidote veins) processes for the actinolite-tremolite formation.

Therefore, to understand the thermobaric environment associated with crystallization of the secondary Act/Tr-bearing paragenesis and to unravel the asbestos-forming processes in Isadalu granitoids, we applied conventional thermobarometric models based on major element mineral chemistry [93–99]. Thermobarometric estimates obtained for secondary actinolite-albite crystallization and for chlorite growth in Isadalu magmatic rocks are  $T = 390\text{--}540 \pm 30$  °C at  $P = 0.55\text{--}1.70 \pm 0.5$  kbar and  $T = 220\text{--}320 \pm 30$  °C, respectively.

Results derived by inverse thermobarometry, together with isotropic fabrics, suggest a P-T range compatible with high-temperature and low-pressure field of the greenschist facies. In particular, results from thermobarometric calculations indicate that Act-bearing paragenesis formed at a very superficial crustal depth of maximum 3–4 km.

The diffuse presence of Qz-veins and Chl + Ep veinlets is compatible with a fluid-rich driven process; furthermore, since dykes cut and are cut by alteration and veins system, it is possible to infer that the hydrothermal activity was coeval to magmatism [105–107] (Figure 5).

Similar to what has been proposed [106,108] for Yerington, Humboldt and Cortez magmatic complexes in Nevada (USA), we can thus state that the Isadalu magmatic complex in Ogliastra shows the metasomatic mineral growth [109] produced during a sodic-calcic (Na + Ca) [106–108,110–112] hydrothermal growth. Na + Ca alteration is typically regional in character [104,109] and could affect extensively all coeval magmatic rocks [106]; it is generally fracture-controlled and alteration envelopes around veins overlaps generating large volumes of pervasively altered rocks [106]. Moreover, areas affected by Na + Ca hydrothermal alteration are usually associated to other alteration types (e.g., [106,112]. All these characteristics are observed in the Isadalu complex and, particularly, in Serra Isadalu hornblende-bearing hypabyssal granitoid rocks where (i) a lower temperature (220–320 °C) Chl + Ep assemblage is representative of propylitic alteration facies and (ii) alteration halos around fractured dykes are recognized.

In the light of the presented results, we can thus conclude that the Isadalu complex represents an example of a magmatic body interested by high-temperature sodic-calcic hydrothermal alteration.

## 6.2. From Fibers to Mountains: A Matter of Hazard

The Isadalu magmatic complex, in Ogliastra (middle–eastern Sardinia) is a Permian volcanic complex at the southern eastern slope of the Gennargentu massif (Figure 4). This complex is located in a highly populated area being surrounded by the three towns of Talana, Villagrande Strisaili and Villanova Strisaili. Serra Isadalu is the main granitoid body with a relief of ca. 1200 masl and is located near the town of Villagrande Strisaili; it constitutes part of the eastern flank of the Bau-Muggeris valley where the dam on the upper Flumendosa river was built between 1940–1950. The dam itself is the first hydroelectric power plant of the Flumendosa river and is named “Primo Salto”, while the artificial man-made lake behind the dam is named “Lago dell’Alto Flumendosa”. This latter lake is the water reservoir for two other hydroelectric plants called “Secondo Salto” and “Terzo Salto”, and constitutes the water supply for irrigation systems used for farming activities in Campidano valley; together with Mulargia Lake, it also represents the water supply for the city of Cagliari and many surrounding minor towns. The pipeline (“condotta di alimentazione” on the map) of the second hydroelectric power plant (Secondo Salto) crosscuts the Bau-Muggeris valley; its penstock is built over the Serra Isadalu granitoid rocks and fall down to its base where the Second Plant is located. Here, the Sa Teula artificial basin collects water, after watermills, and constitutes the reservoir for the Terzo Salto plant. Finally, the Bau-Muggeris valley rocks and the Serra Isadalu granitoids are cut by the Villanova-Villagrande-Talana road system. Moreover, all granitoid rocks from the area have been locally used for house-building in the past.

However, Serra Isadalu together with the other dykes distributed in the Bau-Muggeris are characterized, as outlined in this study, by the presence of acicular to fibrous actinolite-tremolite amphibole due to Na + Ca hydrothermal alteration, thus representing a potential hazard for the environment connected with NOA. Considering only the Serra Isadalu hornblende-bearing hypabyssal granites, having an outcropping volume calculated by topography of ca 0.8–1.0 Km<sup>3</sup>, and assuming a homogeneous primary assemblage texture with ca. 20% in volume of hornblende completely substituted by secondary actinolite-tremolite, the amount of actinolite-tremolite material should be up to 0.16–0.2 km<sup>3</sup>.

We would like to stress that our estimate is only speculative and based on a rough estimation of volumes. Only a detailed geological survey and accurate petrographic investigations could produce reliable results on the actual number of actinolite-tremolite amphiboles in the Isadalu area.

On the other hand, through the combination of field observations, rock-fabric investigations, crystal-morphology and chemical analyses, we clearly demonstrated that actinolite-tremolite fibers might be widespread also in metaluminous Ca-inosilicate-bearing felsic rocks that suffered high temperature sodic-calcic hydrothermal alteration.

## 7. Conclusions

The Isadalu magmatic complex, and in particular its hypabyssal hornblende bearing-felsic rocks, constitute a unique natural laboratory to study NOA fibers in (unexpected) granitoid rocks and to unravel hydrothermal conditions suitable for NOA metasomatic-growth in felsic rocks. The main outcomes that can be extracted from this study are as follows: (i) the metasomatic origin of actinolite-tremolite mineral-bearing paragenesis; (ii) the actinolite-tremolite formation at high-T and low-P conditions (ca. 470 °C and 1 kbar, mean value respectively), and (iii) the capability of sodic-calcic hydrothermal alteration processes to generate NOA amphiboles in felsic/granitoid rocks.

Furthermore, the Isadalu complex is a highly anthropized area, characterized by the presence of three towns (Talana, Villagrande Strisaili, and Villanova Strisaili). In this area, the outcropping NOA-bearing granitoid rocks are the geological background of strategic infrastructures (dams, artificial lake acting as water supply and as water reservoir, pipes of the local hydroelectric plants and local roads) developed since 1948, and all related human activities represent a clear hazard for the environment connected with the NOA. Recent studies show that the fibres pollution in water is increasingly recognized as a potential environmental hazard, totally underestimated up to the present [113,114]. Monitoring the possible presence of NOA in hydrogeological systems sited in rocks enriched in fibrous amphiboles, like the example studied here, is thus mandatory.

Finally, this paper shows that a better knowledge of the genesis and presence of fibrous amphiboles in granitoid rocks may have an impact on future normative and regulations defining environmental hazards due to asbestos occurrences in rocks that have been so far are ignored from this point of view.

**Supplementary Materials:** The following are available online at <http://www.mdpi.com/2075-163X/8/10/442/s1>. The spreadsheet file contains the 4 sheets: (i) Table S1, Complete dataset for the EMPA and chemical formulae of fedlspar from Isadalu magmatic complex; (ii) Table S2, Complete dataset for the EMPA and chemical formulae of epidote from Isadalu magmatic complex; (iii) Table S3, Complete dataset for the EMPA and chemical formulae of chlorite from Isadalu magmatic complex; (iv) Table S4, Complete dataset for the EMPA and chemical formulae of amphibole from Isadalu magmatic complex. This dataset contains all analyses discussed in the text.

**Author Contributions:** Conceptualization, F.L. and G.D.V.; Data curation, F.L., A.C. and M.N.; Formal analysis, F.L. and A.C.; Investigation, F.L., G.D.V., A.C., M.N. and P.S.; Methodology, F.L., G.D.V. and A.C.; Project administration, F.L. and G.D.V.; Resources, F.L., G.D.V., A.C., M.N. and P.S.; Supervision, F.L. and G.D.V.; Validation, F.L. and G.D.V.; Visualization, F.L. and G.D.V.; Writing: original draft, F.L., G.D.V., A.C. and M.N.

**Funding:** This research received no external funding.

**Acknowledgments:** Authors are grateful to three anonymous reviewers and the editor in-house for their helpful comments and suggestions that greatly helped to improve the manuscript. Authors would like to thank Luciano Carta for his help during the first field survey. The Grant to Department of Science, Roma Tre University (MIUR-Italy Dipartimenti di Eccellenza, ARTICOLO 1, COMMI 314–337 LEGGE 232/2016) is gratefully acknowledged.

**Conflicts of Interest:** The authors declare no conflict of interest.

## References

1. Gunter, M.E.; Belluso, E.; Mottana, A. Amphiboles: Environmental and health concerns. *Rev. Mineral. Geochem.* **2007**, *67*, 453–516. [[CrossRef](#)]
2. Vignaroli, G.; Rossetti, F.; Belardi, G.; Billi, A. Linking rock fabric to fibrous mineralisation: A basic tool for the asbestos hazard. *Nat. Hazards Earth Syst. Sci.* **2011**, *11*, 1267–1280. [[CrossRef](#)]



3. Vignaroli, G.; Ballirano, P.; Belardi, G.; Rossetti, F. Asbestos fibre identification vs. evaluation of asbestos hazard in ophiolitic rock mélanges, a case study from the Ligurian Alps (Italy). *Environ. Earth Sci.* **2014**, *72*, 3679–3698. [CrossRef]
4. Martin, R.F. Amphiboles in the igneous environment. *Rev. Mineral. Geochem.* **2007**, *67*, 323–358. [CrossRef]
5. Schulte, P.S.; Trout, D.; Zumwalde, R.D. Asbestos fibers and other elongate mineral particles: State of the science and roadmap for research. In *Current Intelligence Bulletin*; NIOSH: Atlanta, GA, USA, 2011; Volume 62. Available online: <https://stacks.cdc.gov/view/cdc/5892> (accessed on 6 October 2018).
6. Gunter, M.E. Defining asbestos: Differences between the built and natural environments. *Chimia* **2010**, *64*, 747–752. [CrossRef] [PubMed]
7. World Health Organization (WHO). Asbestos and Other Natural Mineral Fibres: Environmental Health Criteria 53. Available online: <http://www.inchem.org/documents/ehc/ehc/ehc53.htm> (accessed on 6 October 2018).
8. Ross, M.; Kuntze, R.A.; Clifton, R.A. A definition for asbestos. In *Definitions for Asbestos and Other Health-Related Silicates*; Levadie, B., Ed.; American Society for Testing and Materials: Philadelphia, PA, USA, 1984; pp. 139–147.
9. Levadie, B. *Definitions for Asbestos and Other Health-Related Silicates: A Symposium (No. 834)*; American Society for Testing and Materials: Philadelphia, PA, USA, 1984.
10. Lee, R.J.; Strohmeier, B.R.; Bunker, K.L.; Van Orden, D.R. Naturally occurring asbestos—A recurring public policy challenge. *J. Hazard. Mater.* **2008**, *153*, 1–21. [CrossRef] [PubMed]
11. Schreier, H. *Asbestos in the Natural Environment*; Elsevier: Amsterdam, The Netherlands, 1989.
12. Lange, J.H.; Lange, P.R.; Reinhard, T.K.; Thomulka, K.W. A study of personal and area airborne asbestos concentrations during asbestos abatement: A statistical evaluation of fibre concentration data. *Ann. Occup. Hyg.* **1996**, *40*, 449–466. [CrossRef]
13. Zakrzewska, A.M.; Capone, P.P.; Iannò, A.; Tarzia, V.; Campopiano, A.; Vilella, E.; Giardino, R. Calabrian ophiolites: Dispersion of airborne asbestos fibers during mining and milling operations. *Period. Mineral.* **2008**, *77*, 27–34.
14. Burilkov, T.; Michailova, L. Asbestos content of the soil and endemic pleural asbestosis. *Environ. Res.* **1970**, *3*, 443–451. [CrossRef]
15. Hardy, R.J.; Highsmith, V.R.; Costa, D.L.; Krewer, J.A. Indoor asbestos concentrations associated with the use of asbestos-contaminated tap water in portable home humidifiers. *Environ. Sci. Technol.* **1992**, *26*, 680–689. [CrossRef]
16. Emmanouil, K.; Kalliopi, A.; Dimitrios, K.; Evangelos, G. Asbestos pollution in an inactive mine: Determination of asbestos fibers in the deposit tailings and water. *J. Hazard. Mater.* **2009**, *167*, 1080–1088.
17. Gualtieri, A.F.; Pollastri, S.; Gandolfi, N.B.; Ronchetti, F.; Albonico, C.; Cavallo, A.; Zanetti, G.; Marini, P.; Sala, O. Determination of the concentration of asbestos minerals in highly contaminated mine tailings: An example from inactive mine waste of Cre'taz and E'marese (Valle d'Aosta, Italy). *Am. Mineral.* **2014**, *99*, 1233–1247. [CrossRef]
18. Bloise, A.; Punturo, R.; Catalano, M.; Miriello, D.; Cirrincione, R. Naturally occurring asbestos (NOA) in rock and soil and relation with human activities: The monitoring example of selected sites in Calabria (southern Italy). *Ital. J. Geosci.* **2016**, *135*, 268–279. [CrossRef]
19. Bellopede, R.; Clerici, C.; Marini, P.; Zanetti, G. Rocks with asbestos: Risk evaluation by means of an abrasion test. *Am. J. Environ. Sci.* **2009**, *5*, 500–506.
20. Giacomini, F.; Boerio, V.; Polattini, S.; Tiepolo, M.; Tribuzio, R.; Zanetti, A. Evaluating asbestos fibre concentration in metaophiolites: A case study from the Voltri Massif and Sestri-Voltaggio Zone (Liguria; NW Italy). *Environ. Earth Sci.* **2010**, *61*, 1621–1639. [CrossRef]
21. Lescano, L.; Marfil, S.; Maiza, P.; Sfragulla, J.; Bonalumi, A. Amphibole in vermiculite mined in Argentina. Morphology; quantitative and chemical studies on the different phases of production and their environmental impact. *Environ. Earth. Sci.* **2013**, *70*, 1809–1821. [CrossRef]
22. Schumacher, J.C. Metamorphic amphiboles: Composition and coexistence. *Rev. Mineral. Geochem.* **2007**, *67*, 359–416. [CrossRef]
23. Ross, M.; Nolan, R.P. History of asbestos discovery and use and asbestos-related disease in context with the occurrence of asbestos within ophiolite complexes. *Geol. Soc. Am.* **2003**, *373*, 447–470.

24. Compagnoni, R.; Groppo, C. Gli amianti in Val di Susa e le rocce che li contengono. *Rend. Soc. Geol. Ital.* **2006**, *3*, 21–28. (In Italian)
25. Van Gosen, B.S. The geology of asbestos in the United States and its practical applications. *Environ. Eng. Geosci.* **2007**, *13*, 55–68. [[CrossRef](#)]
26. Hendrickx, M. Naturally occurring asbestos in eastern Australia: A review of geological occurrence; disturbance and mesothelioma risk. *Environ. Geol.* **2009**, *57*, 909–926. [[CrossRef](#)]
27. Gianfagna, A.; Ballirano, P.; Bellatreccia, F.; Bruni, B.; Paoletti, L.; Oberti, R. Characterization of amphibole fibres linked to mesothelioma in the area of Biancavilla, Eastern Sicily, Italy. *Mineral. Mag.* **2003**, *67*, 1221–1229. [[CrossRef](#)]
28. Strating, E.H.H.; Vissers, R.L. Structures in natural serpentinite gouges. *J. Struct. Geol.* **1994**, *16*, 1205–1215. [[CrossRef](#)]
29. Vissers, R.L.M.; Drury, M.R.; Hoogerduijn, E.H.; Spiers, C.J.; Van der Wal, D. Mantle shear zones and their effect on lithosphere strength during continental breakup. *Tectonophysics* **1995**, *249*, 155–171. [[CrossRef](#)]
30. Scambelluri, M.; Müntener, O.; Hermann, J.; Piccardo, G.B.; Trommsdorff, V. Subduction of water into the mantle: History of an Alpine peridotite. *Geology* **1995**, *23*, 459–462. [[CrossRef](#)]
31. Hermann, J.; Müntener, O.; Scambelluri, M. The importance of serpentinite mylonites for subduction and exhumation of oceanic crust. *Tectonophysics* **2000**, *327*, 225–238. [[CrossRef](#)]
32. Barnes, J.D.; Selverstone, J.; Sharp, Z.D. Interactions between serpentinite devolatilization, metasomatism and strike-slip strain localization during deep-crustal shearing in the Eastern Alps. *J. Metamorph. Geol.* **2004**, *22*, 283–300. [[CrossRef](#)]
33. Li, X.P.; Rahn, M.; Bucher, K. Serpentinites of the Zermatt-Saas ophiolite complex and their texture evolution. *J. Metamorph. Geol.* **2004**, *22*, 159–177. [[CrossRef](#)]
34. Edel, J.B.; Montigny, R.; Thuizat, R. Late Paleozoic rotations of Corsica and Sardinia: New evidence from paleomagnetic and K-Ar studies. *Tectonophysics* **1981**, *79*, 201–223. [[CrossRef](#)]
35. Traversa, G.; Ronca, S.; Del Moro, A.; Pasquali, C.; Buraglini, N.; Barabino, G. Late to post-Hercynian dyke activity in the Sardinia-Corsica domain: A transition from orogenic calc-alkaline to anorogenic alkaline magmatism. *Boll. Soc. Geol. Ital.* **2003**, *2*, 131–152.
36. Edel, J.B. Hypothèse d'une ample rotation horaire tardi-varisque du bloc Maures-Estérel-Corse-Sardaigne. *Géol. Fr.* **2000**, *1*, 3–19. (In French)
37. Atzori, P.; Cirrincione, R.; Del Moro, A.; Mazzoleni, P. Petrogenesis of late Hercynian calc-alkaline dykes of mid-eastern Sardinia: Petrographical and geochemical data constraining hybridization process. *Eur. J. Mineral.* **2000**, *12*, 1261–1282. [[CrossRef](#)]
38. Cortesogno, L.; Cassinis, G.; Dallagiovanna, G.; Gaggero, L.; Oggiano, G.; Ronchi, A.; Seno, S.; Vanossi, M. The Variscan post-collisional volcanism in late Carboniferous–Permian sequences of Ligurian Alps, Southern Alps and Sardinia (Italy): A synthesis. *Lithos* **1998**, *45*, 305–328. [[CrossRef](#)]
39. Carmignani, L.; Carosi, R.; Di Pisa, A.; Gattiglio, M.; Musumeci, G.; Oggiano, G.; Pertusati, P. The hercynian chain in Sardinia (Italy). *Geodin. Acta* **1994**, *7*, 31–47. [[CrossRef](#)]
40. Carmignani, L.; Rossi, P.; Barca, S.; Oggiano, G.; Duran Delga, M.; Salvadori, I.; Conti, P.; Eltrudis, A.; Funedda, A.L.; Pasci, G. *Carta Geologica-Strutturale della Sardegna e della Corsica (Scala 1:500.000)*; BRGM: Orléans, France, 2000.
41. Dini, A.; Di Vincenzo, G.; Ruggieri, G.; Rayner, J.; Lattanzi, P. Monte Ollasteddu, a new gold discovery in the Variscan basement of Sardinia (Italy): First isotopic ( $^{40}\text{Ar}$ - $^{39}\text{Ar}$ , Pb) and fluid inclusion data. *Miner. Depos.* **2005**, *40*, 337–346. [[CrossRef](#)]
42. Ferrara, G.; Ricci, C.; Rita, F. Isotopic ages and tectono-metamorphic history of the metamorphic basement of north-eastern Sardinia. *Contrib. Mineral. Petrol.* **1978**, *68*, 99–106. [[CrossRef](#)]
43. Platt, J.P. Dynamics of orogenic wedges and the uplift of high-pressure metamorphic rocks. *Geol. Soc. Am. Bull.* **1986**, *97*, 1037–1053. [[CrossRef](#)]
44. Elter, F.M.; Faure, M.; Ghezzi, C.; Corsi, B. Les zones de cisaillement tardi-hercyniennes en Sardaigne du Nord-Est (Italie). *Geol. Fr.* **1999**, *2*, 3–16. (In French)
45. Cassinis, G.; Ronchi, A. The (late-) post-Variscan continental succession of Sardinia. *Rend. Soc. Paleontol. Ital.* **2002**, *1*, 77–92.

46. Di Vincenzo, G.; Andriessen, P.A.; Ghezzi, C. Evidence of two different components in a Hercynian peraluminous cordierite-bearing granite: The San Basilio intrusion (central Sardinia; Italy). *J. Petrol.* **1996**, *37*, 1175–1206. [CrossRef]
47. Beccaluva, L.; Civetta, L.; Macciotta, G.; Ricci, C.A. Geochronology in Sardinia: Results and problems. *Rend. Soc. Ital. Min. Petr.* **1985**, *40*, 57–72.
48. Ghezzi, C.; Orsini, J.B. Lineamenti strutturali e composizionali del batolite ercinico sardo-corso in Sardegna. In *Guida alla Geologia del Paleozoico Sardo, Guide Geologiche Regionali*; Chapman & Hall: London, UK, 1982; pp. 88–102.
49. Di Vincenzo, G.; Elter, F.M.; Ghezzi, C.; Palmeri, R.; Ricci, C.A. Petrological evolution of the Palaeozoic basement of Sardinia. In *Petrology, Geology and Ore Deposits of the Palaeozoic Basement of Sardinia; Guide-book to the Field Excursion (B3), Proceedings of the 16th General Meeting of the IMA (4–9 September 1994)*; Ente Minerario Sardo: Cagliari, Italy, 1994; pp. 21–36.
50. Vaccaro, C.; Atzori, P.; Del Moro, A.; Oddone, M.; Traversa, G.; Villa, I.M. Geochronology and Sr-isotope geochemistry of late Hercynian dykes from Sardinia. *Schweiz. Miner. Petrog.* **1991**, *71*, 221–230.
51. Bralio, A.; Ghezzi, C.; Guasparri, G.; Sabatini, G. Aspetti genetici del batolite sardo-corso. *Rend. Soc. Ital. Min. Petr.* **1982**, *38*, 701–764.
52. Ronca, S.; Traversa, G. Late-Hercynian dyke magmatism of Sarrabus (SE Sardinia). *Period. Mineral.* **1996**, *65*, 35–70.
53. Del Moro, A.; Di Simplicio, P.; Ghezzi, C.; Guasparri, G.; Rita, F.; Sabatini, G. Radiometric data and intrusive sequence in the Sardinian batholith. *Neues Jahrb. Mineral. Abh.* **1975**, *126*, 28–44.
54. Atzori, P.; Traversa, G. Post-granitic permo-triassic dyke magmatism in eastern Sardinia (Sarrabus, Barbagia, Mandrolisai, Goceano, Baronie and Gallura). *Period. Mineral.* **1986**, *55*, 203–231.
55. Carmignani, L.; Cherchi, G.P.; Del Moro, A.; Franceschelli, M.; Ghezzi, C.; Musumeci, G.; Pertusati, P.C. The mylonitic granitoids and tectonic units of the Mount Grighini Complex (W-Sardinia): A preliminary note. In *Correlation of Prevariscan and Variscan Events of the Alpine-Mediterranean Mountain Belt*; IGCP project No. 5, Newsletter; UNESCO: Paris, France, 1987; pp. 25–26.
56. Del Moro, A.; Laurenzi, M.; Musumeci, G.; Pardini, G. Geochimica isotopica dello Sr e geocronologia sul complesso intrusivo ercinico del Monte Grighini, Sardegna centro-occidentale. In Proceedings of the Società Italiana di Mineralogia e Petrologia Meeting, Ischia, Italy, 15–18 October 1990. (In Italian)
57. Traversa, G. Sulla giacitura ed età di alcuni filoni basici nelle vulcaniti ignimbriche permiane della Gallura (Sardegna settentrionale). *Rend. Soc. Ital. Min. Petr.* **1969**, *25*, 149–155. (In Italian)
58. Carmignani, L.; Cherchi, A.; Ricci, C.A. Basement structure and Mesozoic-Cenozoic evolution of Sardinia. In *The Lithosphere in Italy*; Boriani, A., Bonafede, M., Piccardo, G.B., Vai, G.B., Eds.; Accademia Nazionale dei Lincei: Roma, Italy, 1989; pp. 63–92.
59. Baldelli, C.; Bigazzi, G.; Elter, F.M.; Macera, P. Description of a permo-trias alkaline lamprophyre embedded into the micaschists of garnet-staurolite-kyanite grade north-eastern Sardinia Island. In Proceedings of the Paleozoic, Stratigraphy, Tectonics, Metamorphism and Magmatism in Italy, Siena, Italy, 13–14 December 1986.
60. Vaccaro, C.; Traversa, G. *REE Distribution in Late Hercynian Dykes from Sardinia*; IGCP N.276, Newsletter; UNESCO: Paris, France, 1992; Volume 5, pp. 215–226.
61. Traversa, G.; Ronca, S.; Pasquali, C. Post-Hercynian basic dyke magmatism of the Concas-Alà dei Sardi alignment (Northern Sardinia-Italy). *Period. Mineral.* **1997**, *66*, 233–262.
62. Cozzupoli, D.; Discendenti, A.; Lombardi, G.; Nicoletti, M. Cronologia K-Ar delle manifestazioni eruttive del settore di Seui-Seulo (Barbagia-Sardegna). *Period. Mineral.* **1971**, *40*, 113–124.
63. Gaggero Sager, L.M.; Cassinis, G.; Cortesogno, L.; Ronchi, A.; Valloni, R. Stratigraphic and Petrographic investigations into the Permian-Triassic continental sequences of Nurra (NWSardinia). *J. Iber. Geol.* **1996**, *21*, 149–170.
64. Lombardi, G.; Cozzupoli, D.; Nicoletti, M. Notizie geopetrografiche e dati sulla cronologia K-Ar del vulcanismo tardopaleozoico sardo. *Period. Mineral.* **1974**, *43*, 221–312.
65. Conti, L.; Maccioni, L.; Pili, P. *Sardegna Scala 1:25.000—Carta Geopetrografica dell'alto Flumendosa (Villanova Strisaili)*; Istituto di Mineralogia e Petrografia, Università di Cagliari; Istituto di Petrografia, Università di Roma—col.-S.E.L.C.A.: Firenze, Italy, 1981; N° inv. 800; Available online: <http://www.geologi.sardegna.it/documenti/cartografia-geologica/> (accessed on 6 October 2018). (In Italian)



66. Zaccaria, B. Saggio di Petrografia: Caratterizzazione Petrografica delle Magmatiti del Mt. Isadalu (Villagrande Strisaili—Ogliastra, Sardegna). In *Tesi Triennale (Unpublished B.S. Thesis)*; Cozzupoli, D., Lucci, F., Eds.; Università degli studi Roma Tre: Roma, Italy, 2010. (In Italian)
67. Lucci, F.; White, J.; Cozzupoli, D.; Traversa, G.; Zaccaria, B. Mt. Isadalu Complex (Sardinia, Italy): An example of post-hercynian transition from High-K calcalkaline to Shoshonitic/Low-K alkaline magmatism. In Proceedings of the Poster presentation at PERALK-CARB Congress, Tuebingen, Germany, 15–16 June 2011.
68. Lucci, F.; White, J.; Campagnola, S. Cpx-Hbl Thermobarometry of Igneous Mafic Rock: Possible History of Permian Andesitic Dyke at Mt. Isadalu Complex (Sardinia, Italy). Poster Presentation at Rittmann Congress 2012. Available online: [https://www.researchgate.net/publication/235347522\\_Cpx-Hbl\\_thermobarometry\\_of\\_igneous\\_mafic\\_rock\\_possible\\_history\\_of\\_Permian\\_andesitic\\_dyke\\_at\\_Mt\\_Isadalu\\_Complex\\_Sardinia\\_Italy](https://www.researchgate.net/publication/235347522_Cpx-Hbl_thermobarometry_of_igneous_mafic_rock_possible_history_of_Permian_andesitic_dyke_at_Mt_Isadalu_Complex_Sardinia_Italy) (accessed on 6 October 2018).
69. Tröger, W.E. *Optical Determination of Rock-forming Minerals—Part 1 Determinative Tables*; English Edition of the Fourth German Edition; Bambauer, H.U., Taborzsky, F., Trochim, H.D., Eds.; E. Schweizerbart'sche Verlagsbuchhandlung (Nägele u. Obermiller): Stuttgart, Germany, 1979.
70. Brandelik, A. CALCMIN—An EXCEL™ Visual Basic application for calculating mineral structural formulae from electron microprobe analyses. *Comput. Geosci.* **2009**, *35*, 1540–1551. [[CrossRef](#)]
71. Vidal, O.; Parra, T.; Vieillard, P. Thermodynamic properties of the Tschermak solid solution in Fe-chlorite: Application to natural examples and possible role of oxidation. *Am. Mineral.* **2005**, *90*, 347–358. [[CrossRef](#)]
72. Locock, A.J. An Excel spreadsheet to classify chemical analyses of amphiboles following the IMA 2012 recommendations. *Comput. Geosci.* **2014**, *62*, 1–11. [[CrossRef](#)]
73. Whitney, D.L.; Evans, B.W. Abbreviations for names of rock-forming minerals. *Am. Mineral.* **2010**, *95*, 185–187. [[CrossRef](#)]
74. Le Maitre, R.W.; Streckeisen, A.; Zanettin, B.; Le Bas, M.J.; Bonin, B.; Bateman, P.; Bellieni, G.; Dudek, A.; Efremova, S.; Keller, J.; et al. *Igneous Rocks: A Classification and Glossary of Terms. Recommendations of the IUGS Subcommission on the Systematics of Igneous Rocks*; Cambridge University Press: Cambridge, UK, 2002.
75. Streckeisen, A.L. Plutonic rock: Classification and nomenclature recommended by the IUGS Subcommission on the Systematics of Igneous Rocks. *Geotimes* **1973**, *18*, 26–30. [[CrossRef](#)]
76. Streckeisen, A. Classification and nomenclature of volcanic rocks, lamprophyres, carbonatites, and melilitic rocks: Recommendations and suggestions of the IUGS Subcommission on the Systematics of Igneous Rocks. *Geology* **1979**, *7*, 331–335. [[CrossRef](#)]
77. Streckeisen, A. To each plutonic rock its proper name. *Earth Sci. Rev.* **1976**, *12*, 1–33. [[CrossRef](#)]
78. Shand, S.J. *Eruptive Rocks*; Murby: London, UK, 1927; p. 360.
79. Shand, S.J. *Eruptive Rocks: Their Genesis, Composition, Classification, and Their Relation to Ore Deposits with a Chapter on Meteorites*; Murby: London, UK, 1943.
80. Shand, S.J. *The Study of Rocks*, 2nd ed.; Murby: London, UK, 1947; p. 236.
81. Millette, J.R. Asbestos analysis methods. In *Asbestos: Risk Assessment, Epidemiology, and Health Effects*; CRC Press: Abingdon, UK, 2006; pp. 9–38.
82. Millette, J.R.; Bandli, B.R. Asbestos identification using available standard methods. *Microscope* **2005**, *53*, 179.
83. Harper, M.; Lee, E.G.; Doorn, S.S.; Hammond, O. Differentiating non-asbestiform amphibole and amphibole asbestos by size characteristics. *J. Occup. Environ. Hyg.* **2008**, *5*, 761–770. [[CrossRef](#)] [[PubMed](#)]
84. Chatfield, E.J. A procedure for quantitative description of fibrosity in amphibole minerals. In Proceedings of the 2008 ASTM Johnson Conference: Critical Issues in Monitoring Asbestos, Burlington, VT, USA, 14–18 July 2008.
85. Rossetti, F.; Nozaem, R.; Lucci, F.; Vignaroli, G.; Gerdes, A.; Nasrabadi, M.; Theye, T. Tectonic setting and geochronology of the Cadomian (Ediacaran-Cambrian) magmatism in central Iran, Kuh-e-Sarhangi region (NW Lut Block). *J. Asian Earth Sci.* **2015**, *102*, 24–44. [[CrossRef](#)]
86. Moghadam, H.S.; Rossetti, F.; Lucci, F.; Chiaradia, M.; Gerdes, A.; Martinez, M.L.; Ghorbani, G.; Nasrabadi, M. The calc-alkaline and adakitic volcanism of the Sabzevar structural zone (NE Iran): Implications for the Eocene magmatic flare-up in Central Iran. *Lithos* **2016**, *248*, 517–535. [[CrossRef](#)]
87. Schmidt, M.W.; Poli, S. Magmatic epidote. *Rev. Mineral. Geochem.* **2004**, *56*, 399–430. [[CrossRef](#)]
88. Hawthorne, F.C.; Oberti, R.; Harlow, G.E.; Maresch, W.V.; Martin, R.F.; Schumacher, J.C.; Welch, M.D. Nomenclature of the amphibole supergroup. *Am. Mineral.* **2012**, *97*, 2031–2048. [[CrossRef](#)]

89. Leake, B.E.; Woolley, A.R.; Arps, C.E.; Birch, W.D.; Gilbert, M.C.; Grice, J.D.; Hawthorne, F.C.; Kato, A.; Kisch, H.J.; Krivovichev, V.G.; et al. Nomenclature of amphiboles: Report of the subcommittee on amphiboles of the international mineralogical association commission on new minerals and mineral names. *Mineral. Mag.* **1997**, *61*, 295–321. [[CrossRef](#)]
90. Leake, B.E.; Woolley, A.R.; Birch, W.D.; Burke, E.A.; Ferraris, G.; Grice, J.D.; Hawthorne, F.C.; Kisch, H.J.; Krivovichev, V.G.; Schumacher, J.C.; et al. Nomenclature of amphiboles: Additions and revisions to the International Mineralogical Association's amphibole nomenclature. *Mineral. Mag.* **2004**, *68*, 209–215. [[CrossRef](#)]
91. Ludwig, K.R. *User's Manual for Isoplot 3.00: A Geochronological Toolkit for Microsoft Excel*; Berkeley Geochronology Center: Berkeley, CA, USA, 2003.
92. Calzolari, G.; Rossetti, F.; Ault, A.K.; Lucci, F.; Olivetti, V.; Nozaem, R. Hematite (U-Th)/He thermochronometry constrains intraplate strike-slip faulting on the Kuh-e-Faghan Fault; central Iran. *Tectonophysics* **2018**, *728*, 41–54. [[CrossRef](#)]
93. Anderson, J.L. Status of thermobarometry in granitic batholiths. *Earth Environ. Sci. Trans. R. Soc. Edinb.* **1996**, *87*, 125–138. [[CrossRef](#)]
94. Anderson, J.L.; Smith, D.R. The effects of temperature and  $fO_2$  on the Al-in-hornblende barometer. *Am. Mineral.* **1995**, *80*, 549–559. [[CrossRef](#)]
95. Schmidt, M.W. Amphibole composition in tonalite as a function of pressure: An experimental calibration of the Al-in-hornblende barometer. *Contrib. Mineral. Petrol.* **1992**, *110*, 304–310. [[CrossRef](#)]
96. Anderson, J.L.; Barth, A.P.; Wooden, J.L.; Mazdab, F. Thermometers and thermobarometers in granitic systems. *Rev. Mineral. Geochem.* **2008**, *69*, 121–142. [[CrossRef](#)]
97. Mutch, E.J.F.; Blundy, J.D.; Tattitch, B.C.; Cooper, F.J.; Brooker, R.A. An experimental study of amphibole stability in low-pressure granitic magmas and a revised Al-in-hornblende geobarometer. *Contrib. Mineral. Petrol.* **2016**, *171*, 85. [[CrossRef](#)]
98. Holland, T.; Blundy, J. Non-ideal interactions in calcic amphiboles and their bearing on amphibole-plagioclase thermometry. *Contrib. Mineral. Petrol.* **1994**, *116*, 433–447. [[CrossRef](#)]
99. Cathelineau, M. Cation site occupancy in chlorites and illites as function of temperature. *Clay Min.* **1988**, *23*, 471–485. [[CrossRef](#)]
100. Rossetti, F.; Asti, R.; Faccenna, C.; Gerdes, A.; Lucci, F.; Theye, T. Magmatism and crustal extension: Constraining activation of the ductile shearing along the Gediz detachment; Menderes Massif (Western Turkey). *Lithos* **2017**, *282*, 145–162. [[CrossRef](#)]
101. Zorpi, M.J.; Coulon, C.; Orsini, J.B. Hybridization between felsic and mafic magmas in calc-alkaline granitoids—A case study in northern Sardinia, Italy. *Chem. Geol.* **1991**, *92*, 45–86. [[CrossRef](#)]
102. Evans, B.W. Metamorphism of alpine peridotite and serpentinite. *Annu. Rev. Earth Planet. Sci.* **1977**, *5*, 397–447. [[CrossRef](#)]
103. Cartwright, I.; Barnicoat, A.C. Geochemical and stable isotope resetting in shear zones from Täschalp: Constraints on fluid flow during exhumation in the Western Alps. *J. Metamorph. Geol.* **2003**, *21*, 143–161. [[CrossRef](#)]
104. Gray, D.R.; Gregory, R.T. Ophiolite obduction and the Samail Ophiolite: The behaviour of the underlying margin. In *Geological Society, London, Special Publications (2003)*; Geological Society of London: London, UK, 2003; Volume 218, pp. 449–465.
105. Dilles, J.H.; Einaudi, M.T. Wall-rock alteration and hydrothermal flow paths about the Ann-Mason porphyry copper deposit, Nevada; a 6-km vertical reconstruction. *Econ. Geol.* **1992**, *87*, 1963–2001. [[CrossRef](#)]
106. Battles, D.A.; Barton, M.D. Arc-related sodic hydrothermal alteration in the western United States. *Geology* **1995**, *23*, 913–916. [[CrossRef](#)]
107. Johnson, D.A.; Barton, M.D.; Hassanzadeh, J. Mafic and felsic hosted Fe-apatite-(REE-Cu) mineralization in Nevada. In *Abstracts with Programs—Geological Society of America*; Geological Society of America: Boulder, CO, USA, 1993; Volume 25, p. 57.
108. Carten, R.B. Sodium-calcium metasomatism, chemical, temporal, and spatial relationships at the Yerington, Nevada; porphyry copper deposit. *Econ. Geol.* **1986**, *81*, 1495–1519. [[CrossRef](#)]
109. Nijland, T.G.; Touret, J.L. Replacement of graphic pegmatite by graphic albite-actinolite-clinopyroxene intergrowths (Mjavatn, southern Norway). *Eur. J. Mineral.* **2001**, *13*, 41–50. [[CrossRef](#)]

110. Mark, G.; Foster, D.R.W. Magmatic–hydrothermal albite–actinolite–apatite-rich rocks from the Cloncurry district, NW Queensland, Australia. *Lithos* **2000**, *51*, 223–245. [[CrossRef](#)]
111. Mark, G.; De Jong, G. Synchronous granitoid emplacement and episodic sodic-calcific alteration in the Cloncurry district: Styles, timing and metallogenic significance. In *New Developments in Metallogenic Research: The McArthur, Mt Isa, Cloncurry Minerals Province*; Baker, T., Rotherham, J., Richmond, J., Mark, G., Williams, P.J., Eds.; James Cook University of North Queensland, Economic Geology Research Unit Contribution: Townsville, Australia, 1996; Volume 5, pp. 81–84.
112. Ridley, J. *Ore Deposit Geology*; Cambridge University Press: Cambridge, UK, 2013.
113. Di Ciaula, A.; Gennaro, V. Rischio clinico da ingestione di fibre di amianto in acqua potabile. *Epidemiol. Prev.* **2016**, *40*, 472–475. (In Italian) [[PubMed](#)]
114. Capuano, F.; Fava, A.; Bacci, T.; Sala, O.; Paoli, F.; Biancolini, V.; Motta, E. La ricerca di amianto nelle acque potabili. *Ecoscienza* **2014**, *3*, 54–55. (In Italian)



© 2018 by the authors. Licensee MDPI, Basel, Switzerland. This article is an open access article distributed under the terms and conditions of the Creative Commons Attribution (CC BY) license (<http://creativecommons.org/licenses/by/4.0/>).